

---

# Structured Neural-PI Control for Networked Systems: Stability and Steady-State Optimality Guarantees

---

Wenqi Cui<sup>1</sup> Yan Jiang<sup>1</sup> Baosen Zhang<sup>1</sup> Yuanyuan Shi<sup>2</sup>

<sup>1</sup>University of Washington, WA 98195 <sup>2</sup>University of California San Diego, CA 92093  
wenqicui@uw.edu jiangyan@uw.edu zhangbao@uw.edu yyshi@eng.ucsd.edu

## Abstract

We study the control of networked systems with the goal of optimizing both transient and steady-state performances while providing stability guarantees. Linear Proportional-Integral (PI) controllers are almost always used in practice, but the linear parameterization of the controller fundamentally limits its performance. Learning-based approaches are becoming popular in designing nonlinear controllers, but the lack of stability guarantees makes the learned controllers difficult to apply in practical applications. This paper bridges the gap between neural network-based controller design and the need for stability guarantees. Using equilibrium-independent passivity, a property present in a wide range of physical systems, we propose structured neural-PI controllers that have provable guarantees on stability and zero steady-state output tracking error. If communication between neighbours is available, we further extend the controller to distributedly achieve optimal resource allocation at the steady state. We explicitly characterize the stability conditions and engineer neural networks that satisfy them by design. Experiments on traffic and power networks demonstrate that the proposed approach can improve both transient and steady-state performances compared to existing state-of-the-art, while unstructured neural networks lead to unstable behaviors.

## 1 Introduction

We study the control of networked physical systems, where a large number of individual subsystems are connected to each other and operate in tandem. Such networked systems are present in numerous applications, and understanding their behaviors has been an active line of research [1–3]. Currently, much of the effort have focused on characterizing properties of the subsystems and their interconnections to certify system stability. At the same time, the performance of these systems, that is, their ability to achieve certain objectives, is also of critical importance. The existing approaches, however, do not offer a framework to optimize system performance.

In this paper, we develop structured neural network-based controllers that not only guarantee stability, but also establishes a framework for performance optimization. In particular, we consider networked systems where the output of the subsystems need to reach an agreement at the steady state [4, 5]. For example, vehicles in a platoon need to reach the same velocity [2] and generators in a power grid need to reach the same speed [6]. This steady state should also be reached as quickly as possible, making transient performance of the system important. At the steady state, we want to select the control that achieves output agreement with the lowest possible cost.

Linear Proportional-Integral (PI) controllers are almost always used in practice to achieve the above goals [7–10]. A proportional term provides instant feedback to improve the transient performance and an integral term drives the system outputs to the desired value at the steady state [7, 8]. If communication is available, previous works [7–11] also tailor the integral term to realize distributed optimal resource allocation under quadratic costs. A linear parameterization, however, fundamentally restricts the degrees of freedom of a controller and can lead to very suboptimal performances.

Learning-based approaches have been proposed to parameterize nonlinear controllers as neural networks, which are then trained to optimize performance [12–15]. However, providing provable guarantees on stability and steady-state optimality has been challenging. In particular, it is nontrivial to certify stability for *all* the possible initial states in a compact set. Recent works showed that monotonic controllers provably stabilize the system [6, 16], but they rely on tailor-made Lyapunov functions and are limited to specific applications.

Moreover, current learning-based approaches generally only optimize transient performance but neglect optimality at the steady-state. Even when training with long time horizons is computationally feasible, it is difficult to quantify how long is enough to cover the steady state. On the other hand, linear PI controllers can achieve stability and steady-state optimality for a large range of systems. This work addresses the following open question: *Can learning be structured to guarantee stability and steady-state optimality for a generalized class of networked systems?*

Clearly, it is not possible to design a controller for everything and the answer depends on picking the right abstraction of the system. Passivity is a classical notion in control theory to characterize the inherent property of dynamical systems by how their inputs and outputs correlate [1]. Many systems have been shown to be equilibrium-independent passive (EIP) [4, 17, 18], which characterize passivity referenced to an arbitrary equilibrium input/output pair. This abstraction allows us to design generalized controllers for networked systems without considering their detailed dynamics.

**Contributions.** This paper focuses on controller design for networked systems where the node dynamics are EIP. We propose a structured neural-PI controller that has provable guarantees on stability and achieves steady-state optimal resource allocation. The key structure we use are monotonically increasing functions, and they are parameterized by what we call *monotone neural networks*. This way, transient performances are optimized by training neural networks, while stability and steady-state optimality are guaranteed by design. Experiments on traffic and power system control demonstrate that the proposed approach can reduce the transient cost by at least 30% compared to the best linear controllers and ensure the optimal steady state cost. Unstructured neural networks, on the other hand, lead to unstable behaviors. We summarize contributions as follows.

- 1) We construct a framework of neural network-based controller design that optimizes both transient and steady-state behavior of networked systems. We adopt a modular approach of stability analysis based on equilibrium-independent passivity, making the framework scalable to large systems and also robust to topology and parameter variations.
- 2) For networked systems without communication, we propose a neural-PI control law that can be implemented fully decentralizedly with only local information. In Theorem 1, we prove that the controller design guarantees asymptotic stability and output agreement at the target value. In Theorem 2, we explicitly characterize the structural conditions of monotone neural networks and prove their universal approximation capability of monotonic functions.
- 3) If a communication network is available, we propose a neural-PI control law where neighbouring nodes can exchange information of their marginal costs. In Theorem 3, we prove that this design guarantees both stability criteria and steady-state optimal resource allocation for a range of functions that includes, but is not restricted to, quadratic cost functions.

## 2 Background and Preliminaries

We consider a networked system as illustrated in Figure 1, where the node dynamics (blue blocks) and the edge dynamics (green blocks) form a closed-loop system by coupling their inputs and outputs through a network. Formally, we define the networked dynamical system on an undirected and connected graph  $\mathcal{G} = (\mathcal{V}, \mathcal{E})$ , consisting of  $n$  nodes,  $\mathcal{V} = \{v_1, \dots, v_n\}$ , and  $m$  edges,  $\mathcal{E} = \{e_1, \dots, e_m\}$ . Each node  $i \in \mathcal{V}$  represents a single-input single-output (SISO) system, for example, a vehicle in Figure 1(b) or a generator in Figure 1(c). Their dynamics are described by:

$$\mathcal{V}_i: \quad \dot{x}_i(t) = f_i(x_i(t), u_i(t)), \quad y_i(t) = h_i(x_i(t)), \quad (1)$$

with state  $x_i(t) \in \mathbb{R}$ , input  $u_i(t) \in \mathbb{R}$ , output  $y_i(t) \in \mathbb{R}$ . We assume the functions  $f_i$  and  $h_i$  are continuous differentiable for all  $i$ . We sometimes omit the time index  $t$  for simplicity. Let  $\mathbf{x} = [x_1, \dots, x_n]^\top$ ,  $\mathbf{y} = [y_1, \dots, y_n]^\top$  and  $\mathbf{u} = [u_1, \dots, u_n]^\top$  for the stacked state, output and input vectors, respectively. The stacked dynamical system is written as  $\dot{\mathbf{x}} = \mathbf{f}(\mathbf{x}, \mathbf{u})$ ,  $\mathbf{y} = \mathbf{h}(\mathbf{x})$ .<sup>1</sup>

<sup>1</sup>Throughout this manuscript, vectors are denoted in lower case bold and matrices are denoted in upper case bold, unless otherwise specified. Vectors of all ones and zeros are denoted as  $\mathbf{1}_n, \mathbf{0}_n \in \mathbb{R}^n$ , respectively.

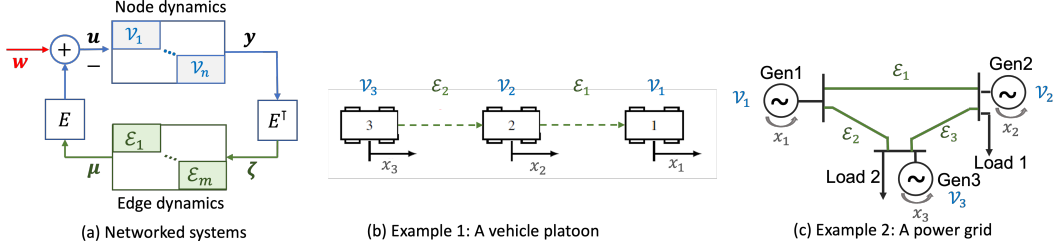


Figure 1: (a) The networked system with node and edge dynamics, the inputs and outputs of the nodes and edges are connected by a graph. The external control input is  $w$ . (b) A vehicle platoon where each node is a vehicle and the edge dynamics describe the relative position between them. (c) A power system where each node is a generator and the edge dynamics are determined by power flow that depends on the angle differences.

The node output  $y$  serves as the input for the edge dynamics. For an edge  $l$  connecting node  $i$  and  $j$ , its input  $\zeta_l(t)$  is the difference in the nodal outputs,  $\zeta_l(t) = y_i(t) - y_j(t)$ . In vector form, we have  $\zeta(t) = E^\top y(t)$ , where  $E \in \mathbb{R}^{n \times m}$  is the incidence matrix such that  $[E]_{i,l}$  has value  $+1$  if node  $i$  is the head of edge  $l$ , and  $-1$  if it is the tail, and  $0$  otherwise. Thus, the edge dynamics are defined by,

$$\mathcal{E}_l : \quad \dot{\eta}_l(t) = \zeta_l(t), \quad \mu_l(t) = \psi_l(\eta_l(t)), \quad (2)$$

with state  $\eta_l(t) \in \mathbb{R}$ , input  $\zeta_l(t) \in \mathbb{R}$ , output  $\mu_l(t) \in \mathbb{R}$ . The function  $\psi_l(\cdot) : \mathbb{R} \mapsto \mathbb{R}$  maps the state  $\eta_l(t)$  of each edge to its output  $\mu_l(t)$ . The edge output  $\mu = \psi(\eta)$  in turn, together with some external control  $w$ , will serve as the input for the node dynamics (1),  $u = -E\psi(\eta) + w$ .

For the networked systems in Figure 1, we wish to achieve two main objectives: 1) fast convergence of system states to the desired operating point; 2) maintaining system operation at the desired point with minimal cost. We will elaborate these objectives in Section 2.1 and Section 2.2. These objectives can be achieved by adjusting the external control  $w$ , and if possible, the edge dynamics  $\psi$ . We provide two motivating examples that fall under our model and will be used in experiments.

**Vehicle platooning.** The first example is the vehicle traffic model in Fig. 1(b), where each node is a vehicle with velocity  $x_i$ , and the edge states  $\eta$  are the relative position between neighbouring vehicles, i.e.,  $\eta_l = x_i - x_j$  [4]. The external control signal  $w$  sets the nominal velocities for the vehicles, and the edge dynamics  $\psi$  controls how each vehicle responds to the observed differences in velocities. The objectives include 1) choose  $w$  and  $\psi$  such that all vehicles reach the same desired velocity; 2) minimizing the fuel consumption of vehicles at this velocity.

**Frequency control in power systems.** The second example is the power system shown in Fig. 1(c), where each node is a generator that rotates with speed (i.e., frequency)  $x_i$ , and the edge states  $\eta$  are the relative angle difference between them,  $\eta_l = x_i - x_j$  [6]. The external control signal  $w$  is the adjustment to generator power outputs. Here the edge dynamics  $\psi$  are determined by physics and are not design variables. The objectives include: 1) choose  $w$  such that each generator reaches the nominal frequency (e.g., 60Hz); 2) minimize the cost of power generation to maintain this frequency.

## 2.1 Stability Criteria

Given a dynamical system in the form of  $\dot{x} = f_u(x)$ , a state  $x^*$  such that  $f_u(x^*) = 0$  is called an equilibrium, where the state variables stop changing. Throughout this paper,  $*$  indicates the equilibrium value of a variable. Next we define the notion of asymptotic stability around an equilibrium.

**Definition 1** (Local Asymptotic Stability). *A dynamical system  $\dot{x} = f_u(x)$  is asymptotically stable around an equilibrium  $x^*$  if,  $\forall \epsilon > 0, \exists \delta > 0$  such that  $\|x(0) - x^*\| < \delta$  ensures  $\|x(t) - x^*\| < \epsilon, \forall t \geq 0$ , and  $\exists \delta' > 0$  such that  $\|x(0) - x^*\| < \delta'$  ensures  $\lim_{t \rightarrow \infty} \|x(t) - x^*\| = 0$ .*

For networked systems described in Figure 1, we are interested in achieving a special type of equilibrium, where the outputs achieve agreement.

**Definition 2** (Output Agreement). *For a networked system  $\mathcal{G} = (\mathcal{V}, \mathcal{E})$  defined with node and edge dynamics (1) and (2), if  $\lim_{t \rightarrow \infty} y_i(t) = \hat{y}$  for all  $i \in \mathcal{V}$ , and  $\hat{y} \in \mathbb{R}$  is a constant, then we say the system reaches output agreement at  $y^* = \hat{y}\mathbb{1}_n$ .*

## 2.2 Optimization Criteria for Transient and Steady-State Performances

In this paper, we propose structured neural network controllers with asymptotic stability and output agreement guarantees, as well as optimize both the transient and steady state performances. A system

is said to be in *steady state* if its states are close to an equilibrium  $\mathbf{x}^*$ , i.e.,  $\forall t \geq T, \|\mathbf{x}(t) - \mathbf{x}^*\| \leq \epsilon$ , where  $\epsilon$  is a small constant. Then the time from 0 to  $T$  is called the *transient period*.

**Transient performance metrics.** During the transient period, our goal is to quickly drive the system to the steady state with the desired agreement value  $\bar{y}$ , while minimizing the external control effort  $\mathbf{w}$ . Let  $J_i$  be the cost function of node  $i$ <sup>2</sup>. The transient optimization problem up to time  $T$  is,

$$\min_{\mathbf{w}} \int_{t=0}^T \sum_{i=1}^n J_i(y_i(t) - \bar{y}, w_i(t)), \quad (3a)$$

$$\text{s.t. dynamics in (1) and (2), stability criteria in Definitions 1 and 2} \quad (3b)$$

In practice, both the cost function  $J_i(\cdot)$  and the system dynamics (1)-(2) can be highly nonlinear and nonconvex. Therefore, the current state-of-the-art is to learn  $\mathbf{w}$  by parameterizing it as a neural network and train it by minimizing the cost in (3a) [19, 20]. But the key challenge with applying these neural network-based controllers is guaranteeing stability [21–23]. Even if the learned policy may appear “stable” during training, it is not necessarily stable during testing. This can be observed in both the vehicle and power system experiments in Section 5.

**Optimal resource allocation at the steady state.** In addition to optimize the transient period performance, we also want to optimize the steady-state cost, i.e. the cost of maintaining the system outputs at the desired value  $\bar{y}\mathbf{1}_n$ . For example, the frequencies in a power system (in North America) should be very close to 60 Hz [24]. Since there are many ways to set generator power output (i.e.,  $\mathbf{w}$ ) to achieve this, the operator needs to find the one that minimizes the generation cost.

Let  $C_i(\cdot)$  be the setpoint cost function for node  $i \in \mathcal{V}$ . The optimal resource allocation problem is,

$$\min_{\mathbf{w}^*} \sum_{i=1}^n C_i(w_i^*), \quad \text{s.t. } \mathbf{y}^* = \bar{y}\mathbf{1}_n, \quad \forall i \in \mathcal{V}. \quad (4)$$

The goal is to enforce that the external control  $\mathbf{w}^*$  at the steady state solves (4), which indicates that the setpoints settle down to the optimal resource allocation solution.

### 2.3 Bridging Controller Design and Stability through Passivity Analysis

To bridge controller design and stability of the networked system, we utilize results in passivity theory. Passivity is a widely adopted tool to analyze stability in control of networked systems [25]. We consider the notion of equilibrium-independent passivity (EIP) [1, 26], which is defined as:

**Definition 3** (Equilibrium-Independent Passivity [1]). *The system described by  $\dot{x}_i = f_i(x_i, u_i)$ ,  $y_i = h_i(x_i)$ ,  $x_i \in \mathcal{X}_i$ ,  $u_i \in \mathcal{U}_i$  is equilibrium-independent passive (EIP) if it satisfies: (i) for every equilibrium  $u_i^* \in \mathcal{U}_i^*$ , there exists a unique  $x_i^* \in \mathcal{X}$  such that  $f_i(x_i^*, u_i^*) = 0$ , and (ii) there exists a positive semidefinite storage function  $W_i(x_i, x_i^*)$  such that*

$$W_i(x_i^*, x_i^*) = 0 \quad \text{and} \quad \dot{W}_i(x_i, x_i^*) \leq (y_i - y_i^*)(u_i - u_i^*). \quad (5)$$

If there further exists a constant  $\rho_i > 0$  such that

$$\dot{W}_i(x_i, x_i^*) \leq -\rho_i \|y_i - y_i^*\|^2 + (y_i - y_i^*)(u_i - u_i^*), \quad (6)$$

then the system is strictly EIP.

The EIP property has been found in a large class of physical systems, including transportation [4], power systems [17, 27], robotics [18], communication [3] and others. Since our goal is to study the stability of the networked system, we make the assumption that each of the subsystems is strictly EIP.

**Assumption 1** (Strict EIP of Nodes). *For all  $i \in \mathcal{V}$ , the nodal dynamic (1) is strictly EIP in  $x_i \in \mathcal{X}_i$ ,  $u_i \in \mathcal{U}_i$  with a storage function  $W_i^{\mathcal{V}}(x_i, x_i^*)$ .*

Passivity plays an important role in stability of a networked system since if we know each component of the system is (strictly) EIP, then the whole system would be stable for a class of controllers and interconnections. Note that an arbitrary interconnection of EIP components does not necessarily lead to a stable system, and it is important to *design* the interconnections and controller to satisfy certain conditions to achieve stability. The rest of the paper characterizes algebraic conditions that the controllers must satisfy and how neural networks can be structured to achieve these conditions.

<sup>2</sup>Including states in the cost function is more cumbersome but does not change the analysis.

### 3 Neural-PI Control with Stability and Output Agreement Guarantees

In this section, we describe the conditions on the edge dynamics  $\psi$ , and external control  $\mathbf{w}$ , that lead to stability of the networked system. Specifically, we show that monotonicity implies stability and output agreement. We then present a neural network architecture that is monotone by construction.

#### 3.1 Generalized PI Control with Stability Implied by Monotonicity

We start by writing the external controller  $\mathbf{w}$  as the following form, for each node  $i \in \mathcal{V}$ ,

$$w_i = p_i(\bar{y}_i - y_i) + r_i(s_i) \quad (7a)$$

$$\dot{s}_i = \bar{y}_i - y_i \quad (7b)$$

At each node  $i$ , the controller is made up of two components. The first component is the proportional term, where  $p_i(\bar{y}_i - y_i)$  is a function of the tracking error between the current output  $y_i$  and desired output  $\bar{y}_i$ . The second component is the integral term, where  $r_i(s_i)$  is a function of the integral of historical tracking errors where  $\dot{s}_i = \bar{y}_i - y_i$ ,  $s_i(0) = 0$ . The above controller follows the structure of the widely adopted Proportional-Integral (PI) controller [28]. Intuitively, the proportional term drives  $y_i$  close to  $\bar{y}_i$  and the integral term drives the accumulated tracking error to zero.

In existing works, linear PI controllers are almost always used [7–10], where  $p_i(\bar{y}_i - y_i) = K_{i,1}(\bar{y}_i - y_i)$ ,  $r_i(s_i) = K_{i,2}s_i$ , and  $K_{i,1}$  and  $K_{i,2}$  are constant coefficients. Linear PI controllers are easy to use and have provable guarantees on stability for a large range of systems. However, their performance can be poor for large-scale nonlinear systems.

Here, we consider a generalized PI controller  $w_i = p_i(\bar{y}_i - y_i) + r_i(s_i)$ , where both control terms are parameterized as neural networks. We then solve the optimal transient performance problem in (3) to find the best network parameters. Neural networks can learn flexible and nonlinear controllers that significantly improve the system performance. Through the following design strategy, we show how to structure the neural networks to provide system stability and output agreement guarantees.

**Controller Design 1** (Stability and Output Agreement Guarantees). *The external control for each node  $i \in \mathcal{V}$  is  $w_i = p_i(\bar{y}_i - y_i) + r_i(s_i)$ , where the functions  $p_i(\cdot)$  and  $r_i(\cdot)$  are Lipschitz continuous and strictly increasing with  $p_i(0) = 0$ ,  $r_i(0) = 0$  for all  $i \in \mathcal{V}$ . In addition, the functions  $\psi_l(\cdot)$  are strictly increasing for all  $l \in \mathcal{E}$ . Compactly, the designed controller is*

$$\mathbf{u} = -\mathbf{E}\psi(\boldsymbol{\eta}) + \mathbf{p}(-\mathbf{y} + \bar{\mathbf{y}}\mathbf{1}_n) + \mathbf{r}(\mathbf{s}) \quad (8a)$$

$$\dot{\mathbf{s}} = -(\mathbf{y} - \bar{\mathbf{y}}\mathbf{1}_n) \quad (8b)$$

The next theorem shows that this design stabilizes the system to a required agreement level  $\bar{\mathbf{y}}\mathbf{1}_n$ .

**Theorem 1.** *Let Assumption 1 holds and the input  $\mathbf{u}$  follows Controller Design 1. If the closed-loop system (1)-(2) has a feasible equilibrium, then the system is locally asymptotically stable around it. In particular, the steady-state outputs converge to  $\bar{\mathbf{y}}$ , namely  $\mathbf{y}^* = \bar{\mathbf{y}}\mathbf{1}_n$ .*

The above controller design features two parts: the external controller  $\mathbf{w}$ , and if possible, the edge dynamics  $\psi(\cdot)$ . The external controller  $\mathbf{w}$  generalizes the linear PI controller, allowing both  $p_i(\cdot)$  and  $r_i(\cdot)$  to be nonlinear functions, as long as they are strictly increasing and cross the origin (these are sometimes called class  $\mathcal{K}$  functions [29]). For systems where we have the design freedom on  $\psi_l(\eta_l)$  (e.g., vehicle platooning in Figure 1 (b)), Controller Design 1 provides the algebraic constraint on the function  $\psi(\cdot)$ . This condition on  $\psi(\cdot)$  is also presented in [2, 4] for networked system without external control. These works, however, did not consider how to choose a good  $\psi(\cdot)$ . The functions  $\psi_l(\eta_l) = \tanh(\eta_l)$  and  $\psi_l(\eta_l) = (\eta_l)^{1/3}$  are used in [4] and [2], respectively. As we show in our experiments, neither are close to being optimal for the transient performance. In Section 3.2, we show how to parameterize neural networks such that these monotonicity conditions can be met, and thus how the controllers and edge dynamics can be optimized through training.

The detailed proof of Theorem 1 is given in Appendix B.1 in the supplementary material, and we sketch the proof here. At an equilibrium, the right side of (8b) equals to zero gives  $\mathbf{y}^* = \bar{\mathbf{y}}\mathbf{1}_n$ . We show this equilibrium is asymptotically stable by constructing a Lyapunov function  $V(\mathbf{x}, \boldsymbol{\eta}, \mathbf{s})$ , that is positive semidefinite and satisfies  $\dot{V}(\mathbf{x}, \boldsymbol{\eta}, \mathbf{s}) \leq 0$  with the equality only holding at the equilibrium. In particular, as shown in the proof, the stability condition does not depend on the specifics of  $f_i(\cdot)$  (as long as it is EIP), making the stability certification robust to parameter changes for networked systems satisfying Assumption 1. We will demonstrate this in the experiment of power system control.

### 3.2 Monotone Neural Network Design

Controller Design 1 requires functions that are monotonically increasing and cross the origin. Technically, this is still an infinite dimensional function space. In this paper, we parameterize these functions by neural networks. The next theorem gives a neural network design in [6, 16] and we rigorously prove that any increasing functions through the origin can be approximated by this construction.

**Theorem 2** (Universal Approximation of Monotonic Functions). *Let  $\alpha^{+(-)} \in \mathbb{R}^d$  and  $\beta^{+(-)} \in \mathbb{R}^d$  be the weights and biases for a single-hidden-layer neural network with  $d$  neurons, where the activation is the ReLU function defined by  $\sigma(z) = \max(z, 0)$ . Let  $\mathcal{Z}$  be an closed interval in  $\mathbb{R}$  and  $r(z) : \mathcal{Z} \mapsto \mathbb{R}$  be a bounded, Lipschitz continuous and monotonically increasing function through the origin. For any  $\epsilon > 0$ , there exists a function  $g(z) : \mathcal{Z} \mapsto \mathbb{R}$  constructed by*

$$g(z) = (\alpha^+)^{\top} \sigma(\mathbb{1}_d z - \beta^+) + (\alpha^-)^{\top} \sigma(-\mathbb{1}_d z + \beta^-) \quad (9a)$$

$$\text{where } -\infty < \sum_{j=1}^d \alpha_j^- < 0 < \sum_{j=1}^d \alpha_j^+ < \infty \quad (9b)$$

$$\beta_d^- \leq \dots \leq \beta_1^- = 0 = \beta_1^+ \leq \dots \leq \beta_d^+, \quad (9c)$$

such that  $|r(z) - g(z)| < \epsilon$  for all  $z \in \mathcal{Z}$ .

The proof of its universal approximation property is provided in Appendix B.2. The constraints in (9b) and (9c) can be easily enforced by an equivalent reparameterization of weights and biases given in Appendix A.2. There are different approaches for designing monotone neural network architectures e.g., [30–32], and any of these could be used to satisfy the conditions in Theorem 1.

## 4 Neural-PI Control for Distributed Optimal Resource Allocation

In this section, we extend the controller design in Section 3 to realize the optimal steady-state resource allocation. Unlike the controller in (7) that only relies on local information, steady-state cost optimization requires communication between neighbours. We reformulate the steady state problem and derive its optimality conditions, and give a distributed algorithm to meet these conditions.

### 4.1 Optimal Resource Allocation at Steady State

To incorporate the optimality condition for the resource allocation problem (4) into controller design, we derive an equivalent formulation for the constraint  $\mathbf{y}^* = \bar{y}\mathbb{1}_n$ . For convenience, we start by explicitly representing the unique mapping from  $u_i^* \in \mathcal{U}_i^*$  to  $x_i^* \in \mathcal{X}$  in Assumption 1.

**Assumption 2** (Equilibrium input-state-output mapping of node dynamics). *For each node  $i \in \mathcal{V}$ , there exists a continuous function  $k_{x,i} : \mathcal{U}_i^* \mapsto \mathcal{X}_i$  for the equilibrium input-state map satisfying  $x_i^* = k_{x,i}(u_i^*)$  and  $f_i(k_{x,i}(u_i^*), u_i^*) = 0$ . Correspondingly, the equilibrium input-output map is defined as the continuous function  $k_{y,i} : \mathcal{U}_i^* \mapsto \mathcal{Y}_i$  with  $k_{y,i}(u_i^*) := h_i(k_{x,i}(u_i^*))$ . Moreover,  $h_i(\cdot)$  and  $k_{x,i}(\cdot)$  are bijective functions, with  $h_i^{-1}(\cdot)$  and  $k_{x,i}^{-1}(\cdot)$  being the inverse functions, respectively.*

The bijective mapping holds broadly for SISO systems and can be easily checked given  $f_i(\cdot)$ . The following lemma gives the optimality conditions for the steady-state resource allocation problem.

**Lemma 1** (Equivalent formulation for optimal resource allocation). *Let Assumption 2 holds and suppose the optimal resource allocation problem (4) has a feasible solution at the output agreement level  $\bar{\mathbf{y}}$ . The optimization problem (4) is equivalent to*

$$\min_{\mathbf{w}^*, \boldsymbol{\mu}^*} \sum_{i=1}^n C_i(w_i^*), \quad (10a)$$

$$\text{s.t. } \mathbf{k}_x^{-1}(\mathbf{h}^{-1}(\bar{\mathbf{y}}\mathbb{1}_n)) = \mathbf{w}^* - \mathbf{E}\boldsymbol{\mu}^*, \quad (10b)$$

where  $\mathbf{w}^*$  is the unique minimizer that satisfies  $\nabla C_i(w_i^*) = \nabla C_j(w_j^*)$ ,  $\forall i, j \in \mathcal{V}$ .

This lemma states that optimality requires  $\mathbf{w}^*$  to reach identical marginal cost, and the detailed proof is given in Appendix B.3 in the supplementary material. To enforce this condition, prior works have

designed distributed averaging-based integral control by communicating the information of  $\nabla C_i(w_i)$  with its neighbours [7–9]. However, they are restricted to quadratic costs and linear controllers. In this paper, we consider nonlinear controllers and a more general class of cost functions.

**Assumption 3** (Scaled-cost gradient functions). *The function  $C_i(\cdot) : \mathbb{R} \mapsto \mathbb{R}$  is strictly convex and continuously differentiable for all  $i \in \mathcal{V}$ . Moreover, there exists a function  $C_o(\cdot) : \mathbb{R} \mapsto \mathbb{R}$  and a group of positive scaling factors  $\mathbf{c} := (c_i, i \in \mathcal{V})$  such that  $\nabla C_i(\cdot) = \nabla C_o(c_i \cdot), \forall i \in \mathcal{V}$ .*

Some examples satisfying Assumption 3 are: 1) *power functions with positive even integer powers:*  $C_i(w_i) = \frac{c_i}{p} w_i^p + b_i$  where  $c_i > 0$  and  $p$  is an even integer (this includes quadratics) 2) *functions that are identical up to constants:*  $C_i(w_i) = C_o(w_i) + b_i$  (e.g., power generators of the same type).

## 4.2 Structured Controller Design

We model communication within the networked system as a connected graph  $\tilde{\mathcal{G}} = (\mathcal{V}, \tilde{\mathcal{E}})$  with an incidence matrix  $\tilde{\mathbf{E}}$ . By adding the communication loop into the integral variable  $\mathbf{s}$ , the integral control term  $\mathbf{r}(\mathbf{s})$  can respond to the difference of marginal costs. The edges in  $\tilde{\mathcal{E}}$  are not necessarily the same as  $\mathcal{E}$  and we use  $\tilde{\cdot}$  to denote all variables belonging to the edges in the communication graph. The communication network associated with nodes of the physical network is designed as follows

$$\mathcal{V}_i : \quad \dot{s}_i = -(y_i - \bar{y}) - c_i q_i, \quad q_i = \sum_{l=1}^m [\tilde{\mathbf{E}}]_{i,l} \tilde{\mu}_l, \quad o_i = \nabla C_i(r_i(s_i)), \quad i \in \mathcal{V} \quad (11a)$$

$$\tilde{\mathcal{E}}_l : \quad \tilde{\zeta}_l = o_i - o_j, \quad \tilde{\mu}_l = \phi_l(\tilde{\zeta}_l), \quad l = (i, j) \in \tilde{\mathcal{E}} \quad (11b)$$

with state  $s_i \in \mathbb{R}$ , input  $q_i \in \mathbb{R}$ , output  $o_i \in \mathbb{R}$  for the nodes, and input  $\tilde{\zeta}_l \in \mathbb{R}$ , output  $\tilde{\mu}_l \in \mathbb{R}$  for the edges. Note that the edges are designed as a memoryless system without states. Compactly, we have the closed-loop dynamics for the communication graph represented by  $\dot{\mathbf{s}} = -(\mathbf{y} - \bar{y}\mathbf{1}_n) - \hat{\mathbf{c}}\tilde{\mathbf{E}}\phi(\tilde{\mathbf{E}}^\top \nabla \mathbf{C}(\mathbf{r}(\mathbf{s})))$ , where  $\hat{\mathbf{c}} = \text{diag}(c_1, \dots, c_n)$ . Then, the control law is designed as follows.

**Controller Design 2** (Distributed Steady-State Optimization). *For each node  $i \in \mathcal{V}$ , the external control law is  $w_i = p_i(\bar{y}_i - y_i) + r_i(s_i)$ , where  $p_i(\cdot)$  and  $r_i(\cdot)$  are Lipschitz continuous and strictly increasing functions with  $p_i(0) = 0$ ,  $r_i(0) = 0$ . The functions  $\psi_l(\cdot)$  are strictly monotonically increasing for all  $l \in \mathcal{E}$ . The ancillary state  $\mathbf{s}$  comes from the communication network (11) where the function  $\phi_l(z) : \mathbb{R} \mapsto \mathbb{R}$  is an odd function and has the same sign as  $z$  for all  $l \in \tilde{\mathcal{E}}$ . Compactly we have the controller design*

$$\mathbf{u} = -\mathbf{E}\psi(\boldsymbol{\eta}) + \mathbf{p}(-\mathbf{y} + \bar{y}\mathbf{1}_n) + \mathbf{r}(\mathbf{s}) \quad (12a)$$

$$\dot{\mathbf{s}} = -(\mathbf{y} - \bar{y}\mathbf{1}_n) - \underbrace{\hat{\mathbf{c}}\tilde{\mathbf{E}}\phi(\tilde{\mathbf{E}}^\top \nabla \mathbf{C}(\mathbf{r}(\mathbf{s})))}_{\text{the term added to (8)}} \quad (12b)$$

The following lemma shows properties of the added term in (12), providing an intuition about why Controller Design 2 can guarantee identical marginal cost (i.e.,  $\nabla \mathbf{C}(\mathbf{r}(\mathbf{s}^*)) \in \text{range}(\mathbf{1}_n)$ ).

**Lemma 2** (Cross term in the communication network). *Suppose Assumption 3 holds. Then*

$$\hat{\mathbf{c}}\tilde{\mathbf{E}}\phi(\tilde{\mathbf{E}}^\top \nabla \mathbf{C}(\mathbf{r}(\mathbf{s}))) = \mathbf{0}_n \quad (13)$$

*if and only if  $\nabla \mathbf{C}(\mathbf{r}(\mathbf{s})) \in \text{range}(\mathbf{1}_n)$ . Moreover,  $\mathbf{r}(\mathbf{s})^\top \hat{\mathbf{c}}\tilde{\mathbf{E}}\phi(\tilde{\mathbf{E}}^\top \nabla \mathbf{C}(\mathbf{r}(\mathbf{s}))) \geq 0$  with equality holds if and only if  $\nabla \mathbf{C}(\mathbf{r}(\mathbf{s})) \in \text{range}(\mathbf{1}_n)$ .*

The proof is given in Appendix B.4 by expanding the terms and the properties of cost functions satisfying Assumption 3. In particular, we use the fact that  $\phi_l(\cdot)$  is an odd function ( $\phi_l(z) = -\phi_l(-z)$ ). We will show in the next subsection that  $\mathbf{y}^* = \bar{y}\mathbf{1}_n$  is maintained and thus  $\mathbf{w}^* = \mathbf{r}(\mathbf{s}^*)$ . Then,  $\nabla \mathbf{C}(\mathbf{r}(\mathbf{s}^*)) \in \text{range}(\mathbf{1}_n)$  is equivalent to  $\nabla \mathbf{C}(\mathbf{w}^*) \in \text{range}(\mathbf{1}_n)$ .

## 4.3 Stability and Steady-State Optimality Guarantee

The next theorem rigorously proves that the closed-loop system (1)-(2) with Controller Design 2 yields an unique equilibrium that guarantees output agreement to  $\bar{y}$  and optimal resources allocation.

**Theorem 3** (Steady-state Optimality). *Let Assumptions 1-3 hold and the input  $\mathbf{u}$  follows the Controller Design 2. Suppose the closed-loop system (1)-(2) has a feasible equilibrium, then it is locally asymptotically stable and uniquely characterized by*

$$\mathbf{y}^* = \bar{y}\mathbf{1}_n, \quad \mathbf{x}^* = \mathbf{h}^{-1}(\bar{y}\mathbf{1}_n), \quad (14a)$$

$$\mathbf{r}(\mathbf{s}^*) = \nabla C_o^{-1}(\gamma)\hat{\mathbf{c}}^{-1}\mathbf{1}_n, \quad (14b)$$

$$-\mathbf{E}\psi(\boldsymbol{\eta}^*) = \mathbf{k}_x^{-1}(\mathbf{h}^{-1}(\bar{y}\mathbf{1}_n)) - \nabla C_o^{-1}(\gamma)\hat{\mathbf{c}}^{-1}\mathbf{1}_n, \quad (14c)$$

where  $\nabla C_o^{-1}(\cdot)$  is the inverse of  $\nabla C_o(\cdot)$  and  $\gamma$  is the unique solution to

$$\nabla C_o^{-1}(\gamma) = -\frac{1}{\bar{c}}\mathbf{1}_n^\top \mathbf{k}_x^{-1}(\mathbf{h}^{-1}(\bar{y}\mathbf{1}_n)), \quad \bar{c} = \left( \sum_{i=1}^n c_i^{-1} \right). \quad (15)$$

In particular,  $\mathbf{w}^* = \mathbf{r}(\mathbf{s}^*)$  and  $\nabla C_i(w_i^*) = \nabla C_j(w_j^*)$ ,  $\forall i, j \in \mathcal{V}$ . That is, the equilibrium solves the optimal resource allocation problem (10).

The proof is given in Appendix B.5. The key steps follow the equality at equilibrium and conditions in Lemma 2. Asymptotically stability is proved using the same Lyapunov function as in Theorem 1.

## 5 Experiments

We end the paper with case studies demonstrating the effectiveness the proposed neural-PI control in two networked systems: vehicle platooning and power system frequency control. All experiments are run with a NVIDIA Tesla P100 GPU with 16GB memory. The proposed neural PI controller can be trained by any model-based or model-free algorithms, and we use the RNN-based framework in [6, 33] for training. Detailed problem formulation, verification of assumptions, simulation setting and results are provided in Appendix C.1 and C.2 in the supplementary material. We briefly highlight some of the key observations below. Code for all experiments are available at [https://github.com/Wenqi-Cui/NeuralPI\\_Networked\\_Systems](https://github.com/Wenqi-Cui/NeuralPI_Networked_Systems).

### 5.1 Vehicle Platooning

**Experiment Setup.** We conduct experiments on the platooning problem in Figure 1(b) with 20 vehicles ( $n = 20$ ), where the node states  $\mathbf{x}$  are the velocities and the edge states  $\boldsymbol{\eta}$  are the relative positions between neighbouring vehicles [2, 4]. The vehicles need to reach the same velocity to avoid possible collisions. There are two design freedoms: 1) the feedback function  $\psi_l(\eta_l)$  and 2) adjustments to the preferred velocity  $w_i$ . Cost is defined as  $C(\mathbf{w}^*) = \sum_{i=1}^n c_i (w_i^*)^2$ , where  $c_i \sim \text{uniform}[0.025, 0.075]$ . We generate the training and test set of size 300 with initial velocities  $x_0 \sim \text{uniform}[5, 6]$ .

**Learning Edge Feedback Function.** We first demonstrate the performance of the learned edge feedback function  $\psi_l(\cdot)$ , for systems without external control  $\mathbf{w}$ . Figure 2 compares the performance of  $\psi_l(\cdot)$  parameterized by neural networks (labeled as StableNN) with  $\tanh(\eta_l - \eta_0)$  in [4] and  $(\eta_l - \eta_0)^{1/3}$  (labeled as poly1/3) in [2], where  $\eta_0 = 2$  is the initial distance of neighbouring vehicles. The shape of different edge feedback functions is shown in Figure 2(a), where StableNN learns a monotonically increasing function with flexible shape. Figure 2(b)-(d) visualize the transient velocity of all vehicles from the same initial condition. All of the dynamics reach an output agreement, with StableNN realizes better transient performance with quick convergence.

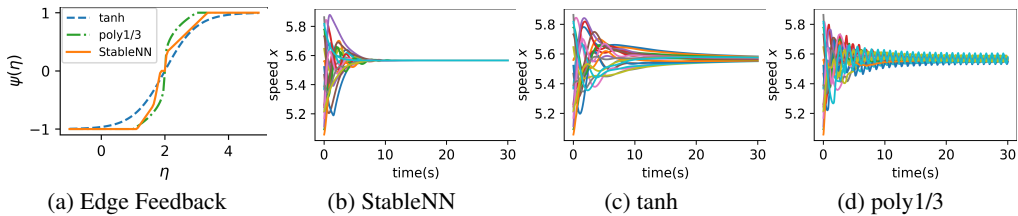


Figure 2: (a) The edge feedback functions learned by StableNN compared to tanh and poly1/3. (b)-(d) System dynamics with different edge feedback functions. The system with StableNN converges the quickest.



**Controller Performance.** We compare the performance of the learned structured neural-PI controllers, 1) StableNN-Comm, the neural-PI controller with communication (Controller design 2) and, 2) StableNN-WoComm, the neural-PI controller without communication (Controller Design 1). Both neural-PI controllers are parameterized by monotone neural networks given in Theorem 2. We compare against two benchmarks with communication: 3) DenseNN-Comm: Dense neural networks with ReLU activation, 4) Linear-Comm: linear PI control. Figure 3(a) shows the transient and steady-state costs on the test set. StableNN-Comm and Linear-Comm has the lowest possible steady-state cost, as guaranteed by Theorem 3. Figure 3(b) and 3(c) show the dynamics of selected nodes under DenseNN-Comm and StableNN-Comm, respectively. Even through DenseNN achieves finite loss both in training and testing, node 3 actually exhibits unstable behavior. By contrast, the neural-PI controller achieves agreement at  $\bar{y} = 5.2$  with the minimum cost.

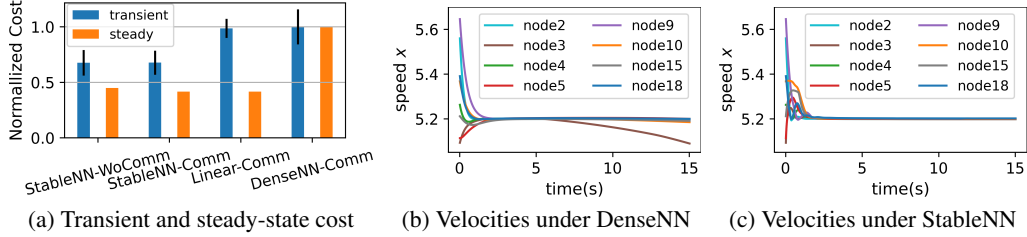


Figure 3: (a) The average transient cost and steady-state cost with error bar on the randomly generated test set. (b) The dynamics of DenseNN-Comm. (c) The dynamics of StableNN-Comm

## 5.2 Power Systems Frequency Control

**Experiment Setup.** The second experiment is the power system frequency control on the IEEE 39-bus New England system [34]. For this case, the edge feedback is determined by the physical law of power flow  $\psi_l(\eta_l) = \sin(\eta_l)$ . Here, we choose  $\mathbf{w}$  such that the generators reach the required speed 60Hz at the steady state and minimize the cost of power generation represented by  $C(\mathbf{w}^*) = \sum_{i=1}^n c_i (w_i^*)^4$ , where  $c_i \sim \text{uniform}[0.5, 1.5]$ . The load at bus  $i$  is a parameter in the function  $f_i(\cdot)$ .

**Robustness to Parameter Changes.** We generate the training and test set of size 300 with random loads to verify that the proposed controller design is robust to parameter changes. The transient and steady-state costs on the test set (with different load levels) are illustrated in Figure 4(a). StableNN-Comm achieves the lowest transient and steady-state cost. Linear-Comm achieves optimal steady-state cost, but has poor transient behavior and StableNN-WoComm has good transient cost but does not converge to the optimal steady state solution. Again, DenseNN-Comm without the guarantees in Controller Designs 1 and 2 is unstable (Figure 4(b)).

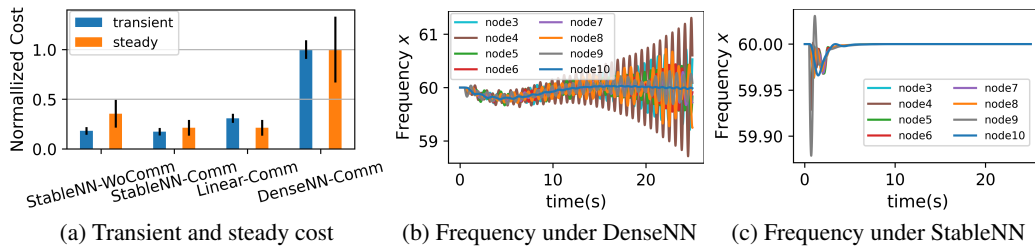


Figure 4: (a) The average transient and steady-state cost with error bar on the test set with random load changes. (b) The dynamics of DenseNN-Comm. (c) The dynamics of StableNN-Comm.

## 6 Conclusions

This paper proposed structured Neural-PI controllers for networked systems where node dynamics are equilibrium independently passive. The proposed controllers have provable guarantees on stability and can distributedly achieve optimal resource allocation at the steady state. Experiments demonstrate that the proposed approach can improve both transient and steady-state performances and is also robust to parameter changes, while unstructured neural networks lead to unstable behaviors. Important future directions include relaxing the limitations on the one-dimensional SISO nodal system and incorporating other safety constraints.

## References

- [1] Murat Arcak, Chris Meissen, and Andrew Packard. *Networks of dissipative systems: compositional certification of stability, performance, and safety*. Springer, 2016.
- [2] Samuel Coogan and Murat Arcak. A dissipativity approach to safety verification for interconnected systems. *IEEE Transactions on Automatic Control*, 60(6):1722–1727, 2014.
- [3] John W Simpson-Porco. Equilibrium-independent dissipativity with quadratic supply rates. *IEEE Transactions on Automatic Control*, 64(4):1440–1455, 2018.
- [4] Mathias Bürger, Daniel Zelazo, and Frank Allgöwer. Duality and network theory in passivity-based cooperative control. *Automatica*, 50(8):2051–2061, 2014.
- [5] Florian Dörfler and Francesco Bullo. Synchronization in complex networks of phase oscillators: A survey. *Automatica*, 50(6):1539–1564, 2014.
- [6] Wenqi Cui, Yan Jiang, and Baosen Zhang. Reinforcement learning for optimal primary frequency control: A Lyapunov approach. *IEEE Transaction on Power Systems*, 2022.
- [7] Changhong Zhao, Enrique Mallada, and Florian Dörfler. Distributed frequency control for stability and economic dispatch in power networks. In *Proc. of American Control Conference*, pages 2359–2364, July 2015. doi: 10.1109/ACC.2015.7171085.
- [8] Martin Andreasson, Dimos V Dimarogonas, Henrik Sandberg, and Karl Henrik Johansson. Distributed control of networked dynamical systems: Static feedback, integral action and consensus. *IEEE Transactions on Automatic Control*, 59(7):1750–1764, 2014.
- [9] Erik Weitenberg, Claudio De Persis, and Nima Monshizadeh. Exponential convergence under distributed averaging integral frequency control. *Automatica*, 98:103–113, Dec. 2018.
- [10] Farid Golnaraghi and Benjamin C Kuo. *Automatic control systems*. McGraw-Hill Education, 2017.
- [11] Johannes Schiffer, Florian Dörfler, and Emilia Fridman. Robustness of distributed averaging control in power systems: Time delays & dynamic communication topology. *Automatica*, 80: 261–271, June 2017. ISSN 0005-1098. doi: <https://doi.org/10.1016/j.automatica.2017.02.040>.
- [12] Kaiqing Zhang, Zhuoran Yang, and Tamer Başar. Multi-agent reinforcement learning: A selective overview of theories and algorithms. *Handbook of Reinforcement Learning and Control*, pages 321–384, 2021.
- [13] Guannan Qu, Yiheng Lin, Adam Wierman, and Na Li. Scalable multi-agent reinforcement learning for networked systems with average reward. *Advances in Neural Information Processing Systems*, 33:2074–2086, 2020.
- [14] Jianhong Wang, Wangkun Xu, Yunjie Gu, Wenbin Song, and Tim C Green. Multi-agent reinforcement learning for active voltage control on power distribution networks. *Advances in Neural Information Processing Systems*, 34:3271–3284, 2021.
- [15] Tianshu Chu, Sandeep Chinchali, and Sachin Katti. Multi-agent reinforcement learning for networked system control. In *International Conference on Learning Representations*, 2019.
- [16] Yuanyuan Shi, Guannan Qu, Steven Low, Anima Anandkumar, and Adam Wierman. Stability constrained reinforcement learning for real-time voltage control. *American Control Conference (ACC)*, 2022.
- [17] Wenqi Cui and Baosen Zhang. Equilibrium-independent stability analysis for distribution systems with lossy transmission lines. *arXiv preprint arXiv:2203.04580*, 2022.
- [18] Chris Meissen, Kristian Klausen, Murat Arcak, Thor I Fossen, and Andrew Packard. Passivity-based formation control for uavs with a suspended load. *IFAC-PapersOnLine*, 50(1):13150–13155, 2017.
- [19] Anusha Nagabandi, Gregory Kahn, Ronald S Fearing, and Sergey Levine. Neural network dynamics for model-based deep reinforcement learning with model-free fine-tuning. In *2018 IEEE International Conference on Robotics and Automation (ICRA)*, pages 7559–7566. IEEE, 2018.
- [20] Lucian Buşoniu, Tim de Bruin, Domagoj Tolić, Jens Kober, and Ivana Palunko. Reinforcement learning for control: Performance, stability, and deep approximators. *Annual Reviews in Control*, 46:8–28, 2018.

- [21] Priya L Donti, Melrose Roderick, Mahyar Fazlyab, and J Zico Kolter. Enforcing robust control guarantees within neural network policies. In *International Conference on Learning Representations*, 2020.
- [22] Ya-Chien Chang, Nima Roohi, and Sicun Gao. Neural lyapunov control. *Advances in neural information processing systems*, 32, 2019.
- [23] Wanxin Jin, Zhaoran Wang, Zhuoran Yang, and Shaoshuai Mou. Neural certificates for safe control policies. *arXiv preprint arXiv:2006.08465*, 2020.
- [24] Peter W Sauer, Mangalore A Pai, and Joe H Chow. *Power system dynamics and stability: with synchrophasor measurement and power system toolbox*. John Wiley & Sons, 2017.
- [25] Jean-Jacques E Slotine, Weiping Li, et al. *Applied nonlinear control*, volume 199. Prentice hall Englewood Cliffs, NJ, 1991.
- [26] George H Hines, Murat Arcak, and Andrew K Packard. Equilibrium-independent passivity: A new definition and numerical certification. *Automatica*, 47(9):1949–1956, 2011.
- [27] Pulkit Nahata, Raffaele Soloperto, Michele Tucci, Andrea Martinelli, and Giancarlo Ferrari-Trecate. A passivity-based approach to voltage stabilization in dc microgrids with zip loads. *Automatica*, 113:108770, 2020.
- [28] Karl Johan Åström, Tore Hägglund, and Karl J Astrom. *Advanced PID control*, volume 461. ISA-The Instrumentation, Systems, and Automation Society Research Triangle Park, 2006.
- [29] Murat Arcak and Andrew Teel. Input-to-state stability for a class of lurie systems. *Automatica*, 38(11):1945–1949, 2002.
- [30] Joseph Sill. Monotonic networks. In *Proceedings of the 10th International Conference on Neural Information Processing Systems*, pages 661–667, 1997.
- [31] Antoine Wehenkel and Gilles Louppe. Unconstrained monotonic neural networks. *Advances in neural information processing systems*, 32, 2019.
- [32] Xingchao Liu, Xing Han, Na Zhang, and Qiang Liu. Certified monotonic neural networks. *Advances in Neural Information Processing Systems*, 33:15427–15438, 2020.
- [33] Ján Drgona, Aaron Tuor, and Draguna Vrabie. Learning constrained adaptive differentiable predictive control policies with guarantees. *arXiv preprint arXiv:2004.11184*, 2020.
- [34] T Athay, Robin Podmore, and Sudhir Virmani. A practical method for the direct analysis of transient stability. *IEEE Transactions on Power Apparatus and Systems*, (2):573–584, 1979.
- [35] H. K. Khalil. *Nonlinear Systems*. Prentice Hall, 3rd edition, 2002.
- [36] Stephen Boyd and Lieven Vandenberghe. *Convex Optimization*. Cambridge University Press, 2004.
- [37] Norman Biggs, Norman Linstead Biggs, and Biggs Norman. *Algebraic graph theory*. Number 67. Cambridge university press, 1993.
- [38] R. Tyrrell Rockafellar and Roger J. B. Wets. *Variational Analysis*. Springer, 1998.
- [39] Prabha Kundur, Neal J Balu, and Mark G Lauby. *Power system stability and control*, volume 7. McGraw-hill New York, 1994.
- [40] Erik Weitenberg, Yan Jiang, Changhong Zhao, Enrique Mallada, Claudio De Persis, and Florian Dörfler. Robust decentralized secondary frequency control in power systems: Merits and tradeoffs. *IEEE Transactions on Automatic Control*, 64(10):3967–3982, Oct. 2019.
- [41] Florian Dörfler and Sergio Grammatico. Gather-and-broadcast frequency control in power systems. *Automatica*, 79:296–305, May 2017. ISSN 0005-1098. doi: <https://doi.org/10.1016/j.automatica.2017.02.003>.

## A Review of Existing Results

### A.1 Lyapunov's Direct Method for Proving Asymptotic Stability

Throughout the paper, we prove asymptotic stability using Lyapunov's direct method [35] shown as follows.

**Proposition 1** (Lyapunov functions and asymptotic stability). *Consider a controlled system  $\dot{\mathbf{x}} = \mathbf{f}_u(\mathbf{x})$ ,  $\mathbf{x} \in \mathcal{X}$  with equilibrium at  $\mathbf{x}^* \in \mathcal{X}$ . Suppose there exists a continuously differentiable function  $V : \mathcal{X} \mapsto \mathbb{R}$  that satisfies the following conditions*

$$V(\mathbf{x}) > 0 \quad \forall \mathbf{x} \in \mathcal{X} \setminus \mathbf{x}^* \quad (16a)$$

$$\dot{V}(\mathbf{x}) = (\nabla_{\mathbf{x}} V(\mathbf{x}))^\top \dot{\mathbf{x}} < 0 \quad \forall \mathbf{x} \in \mathcal{X} \setminus \mathbf{x}^* \quad (16b)$$

$$V(\mathbf{x}^*) = 0, \quad \dot{V}(\mathbf{x}^*) = 0, \quad (16c)$$

Then the system is asymptotically stable at the equilibrium.

The key to show stability is to construct a Lyapunov function and verify the satisfaction of the conditions in Proposition 1.

### A.2 Implementation of the Monotone Neural Network in Theorem 2

The constraints in (9b) and (9c) are not trivial to enforce when training the neural network. We adopt the trick in [6, 16] to address this challenge. Specifically, we introduce a group of intermediate parameters  $\tilde{\alpha}^{+(-)} \in \mathbb{R}^d$  and  $\tilde{\beta}^{+(-)} \in \mathbb{R}^{d-1}$  that are unconstrained such that the original parameters  $\alpha^{+(-)} \in \mathbb{R}^{d-1}$  and  $\beta^{+(-)} \in \mathbb{R}^d$  are parameterized as

$$\begin{aligned} \alpha_1^+ &= (\tilde{\alpha}_1^+)^2, & \alpha_j^+ &= (\tilde{\alpha}_j^+)^2 - (\tilde{\alpha}_{j-1}^+)^2, \forall j = 2, \dots, d \\ \alpha_1^- &= -(\tilde{\alpha}_1^-)^2, & \alpha_j^- &= -(\tilde{\alpha}_j^-)^2 + (\tilde{\alpha}_{j-1}^-)^2, \forall j = 2, \dots, d \\ \beta_1^+ &= 0, & \beta_j^+ &= \sum_{i=1}^{j-1} (\tilde{\beta}_i^+)^2, \forall j = 2, \dots, d \\ \beta_1^- &= 0, & \beta_j^- &= -\sum_{i=1}^{j-1} (\tilde{\beta}_i^-)^2, \forall j = 2, \dots, d. \end{aligned} \quad (17)$$

By inspection, (9b) and (9c) naturally hold through the construction in (17).

In training, the back-propagation is conducted with respect to weights  $\tilde{\alpha}^+ \in \mathbb{R}^d$ ,  $\tilde{\alpha}^- \in \mathbb{R}^d$ ,  $\tilde{\beta}^+ \in \mathbb{R}^{d-1}$ ,  $\tilde{\beta}^- \in \mathbb{R}^{d-1}$ . Then the monotonic function in Section 3.2 is implemented using the pseudo-code in Algorithm 1. It realizes a function  $g(z)$  that is monotonically increasing and cross the origin. We use this construction for each monotonic functions in the Controller Design 1 and Controller Design 2.

---

#### Algorithm 1 Monotone Neural Network with Stacked ReLU Functions

---

**Input:** Variable  $z$ , Weights  $\tilde{\alpha}^+ \in \mathbb{R}^d$ ,  $\tilde{\alpha}^- \in \mathbb{R}^d$ ,  $\tilde{\beta}^+ \in \mathbb{R}^{d-1}$ ,  $\tilde{\beta}^- \in \mathbb{R}^{d-1}$

Set up the value for the first neuron  $\alpha_1^+ = (\tilde{\alpha}_1^+)^2$ ,  $\alpha_1^- = -(\tilde{\alpha}_1^-)^2$ ,  $\beta_1^+ = 0$ ,  $\beta_1^- = 0$

1: **for**  $j = 2$  to  $d$  **do**

2:  $\alpha_j^+ = (\tilde{\alpha}_j^+)^2 - (\tilde{\alpha}_{j-1}^+)^2$ ,  $\alpha_j^- = -(\tilde{\alpha}_j^-)^2 + (\tilde{\alpha}_{j-1}^-)^2$

3:  $\beta_j^+ = \sum_{i=1}^{j-1} (\tilde{\beta}_i^+)^2$ ,  $\beta_j^- = -\sum_{i=1}^{j-1} (\tilde{\beta}_i^-)^2$

4: **end for**

**Output:**  $g(z) = (\alpha^+)^{\top} \sigma(\mathbf{1}_d z - \beta^+) + (\alpha^-)^{\top} \sigma(-\mathbf{1}_d z + \beta^-)$

---

## B Proof

### B.1 Proof of Theorem 1

We first derive conditions at an equilibrium to show the output agreement at the required level. Then, we prove that the system is locally asymptotically stable around an equilibrium.

At the equilibrium, the right side of (8b) equals to zero gives  $\mathbf{y}^* = \bar{y}\mathbf{1}_n$ . Correspondingly,  $p_i(\bar{y}_i - y_i^*) = 0$ . By the well-defined bijective mapping in Assumption 2, we further have  $\mathbf{x}^* = \mathbf{h}^{-1}(\bar{y}\mathbf{1}_n)$  and the input equals to  $\mathbf{u}^* = \mathbf{k}_x^{-1}(\mathbf{h}^{-1}(\bar{y}\mathbf{1}_n))$ . Hence,  $-\mathbf{E}\boldsymbol{\mu}^* + \mathbf{r}(\mathbf{s}^*) + \mathbf{p}(-\mathbf{y}^* + \bar{y}\mathbf{1}_n) = \mathbf{k}_x^{-1}(\mathbf{h}^{-1}(\bar{y}\mathbf{1}_n))$ , where  $\mathbf{p}(-\mathbf{y}^* + \bar{y}\mathbf{1}_n) = 0$  when  $\mathbf{y}^* = \bar{y}\mathbf{1}_n$ . The set of state variables at equilibrium is given by  $\mathcal{S}_e = \{\mathbf{x}^*, \boldsymbol{\eta}^*, \mathbf{s}^* | \mathbf{x}^* = \mathbf{h}^{-1}(\bar{y}\mathbf{1}_n), \mathbf{r}(\mathbf{s}^*) - \mathbf{E}\boldsymbol{\psi}(\boldsymbol{\eta}^*) = \mathbf{k}_x^{-1}(\mathbf{h}^{-1}(\bar{y}\mathbf{1}_n))\}$ . It should be noted that the set  $\mathcal{S}_e$  is not always nonempty and whether a feasible equilibrium exists can be checked after the functions  $\mathbf{f}(\cdot)$ ,  $\mathbf{h}(\cdot)$  are specified.

Next, we construct a Lyapunov function to prove that if there is a feasible equilibrium in  $\mathcal{S}_e$ , then the system is locally asymptotically stable around it. Define the integral function  $L(\mathbf{s}) := \sum_{i=1}^n \int_0^{s_i} r_i(z) dz$ , which is convex since  $\nabla^2 L(\mathbf{s}) = \text{diag}(r'_1(s_1), \dots, r'_n(s_n)) \succ 0$  by the strictly increasing design of  $r_i(\cdot)$  for all  $i$ . Correspondingly, the Bregman distance defined by

$$B^{\mathcal{V}}(\mathbf{s}, \mathbf{s}^*) = L(\mathbf{s}) - L(\mathbf{s}^*) - \nabla L(\mathbf{s}^*)^\top (\mathbf{s} - \mathbf{s}^*)$$

is positive definite with equality holds if and only if  $\mathbf{s} = \mathbf{s}^*$  [36].

Following the same line of proof, the integral functions  $Q(\boldsymbol{\eta}) = \sum_{l=1}^m \int_0^{\eta_l} \psi_l(z) dz$  is also convex. Correspondingly, the Bregman distance defined by:

$$B^{\mathcal{E}}(\boldsymbol{\eta}, \boldsymbol{\eta}^*) = Q(\boldsymbol{\eta}) - Q(\boldsymbol{\eta}^*) - \nabla Q(\boldsymbol{\eta}^*) (\boldsymbol{\eta} - \boldsymbol{\eta}^*).$$

is positive definite with equality holds if and only if  $\boldsymbol{\eta} = \boldsymbol{\eta}^*$  [36].

We construct a Lyapunov function as

$$V(\mathbf{x}, \boldsymbol{\eta}, \mathbf{s})|_{\mathbf{x}^*, \boldsymbol{\eta}^*, \mathbf{s}^*} = \sum_{i=1}^n W_i^{\mathcal{V}}(x_i, x_i^*) + B^{\mathcal{E}}(\boldsymbol{\eta}, \boldsymbol{\eta}^*) + B^{\mathcal{V}}(\mathbf{s}, \mathbf{s}^*), \quad (18)$$

where the functions by construction satisfies  $\sum_{i=1}^n W_i^{\mathcal{V}}(x_i, x_i^*) \geq 0$ ,  $B^{\mathcal{E}}(\boldsymbol{\eta}, \boldsymbol{\eta}^*) \geq 0$ ,  $B^{\mathcal{V}}(\mathbf{s}, \mathbf{s}^*) \geq 0$  with equality holds only when  $\mathbf{x} = \mathbf{x}^*$ ,  $\boldsymbol{\eta} = \boldsymbol{\eta}^*$ , and  $\mathbf{s} = \mathbf{s}^*$ , respectively. Hence,  $V(\mathbf{x}, \boldsymbol{\eta}, \mathbf{s})|_{\mathbf{x}^*, \boldsymbol{\eta}^*, \mathbf{s}^*}$  is a well-defined function that is positive definite and equals to zero at the equilibrium.

To prepare for the calculation of the time derivative of the Lyapunov function, we start by calculating the time derivative of functions  $B^{\mathcal{V}}(\mathbf{s}, \mathbf{s}^*)$  and  $B^{\mathcal{E}}(\boldsymbol{\eta}, \boldsymbol{\eta}^*)$ . The time derivative of  $B^{\mathcal{V}}(\mathbf{s}, \mathbf{s}^*)$  is

$$\begin{aligned} \dot{B}^{\mathcal{V}}(\mathbf{s}, \mathbf{s}^*) &= (\nabla L(\mathbf{s}) - \nabla L(\mathbf{s}^*))^\top \dot{\mathbf{s}} \\ &\stackrel{\textcircled{1}}{=} (\mathbf{r}(\mathbf{s}) + \mathbf{r}(\mathbf{s}^*))^\top (-\mathbf{y} - \mathbf{y}^*), \end{aligned} \quad (19)$$

where  $\textcircled{1}$  follows from  $\nabla L(\boldsymbol{\eta}) = \mathbf{r}(\mathbf{s})$  and  $\dot{\mathbf{s}} = -(\mathbf{y} - \bar{y}\mathbf{1}_n) = -(\mathbf{y} - \mathbf{y}^*)$  by definition.

The time derivative of  $B^{\mathcal{E}}(\boldsymbol{\eta}, \boldsymbol{\eta}^*)$  is

$$\begin{aligned} \dot{B}^{\mathcal{E}}(\boldsymbol{\eta}, \boldsymbol{\eta}^*) &= (\nabla Q(\boldsymbol{\eta}) - \nabla Q(\boldsymbol{\eta}^*))^\top \dot{\boldsymbol{\eta}} \\ &\stackrel{\textcircled{1}}{=} (\boldsymbol{\psi}(\boldsymbol{\eta}) - \boldsymbol{\psi}(\boldsymbol{\eta}^*))^\top \boldsymbol{\zeta} \\ &\stackrel{\textcircled{2}}{=} (\boldsymbol{\mu} - \boldsymbol{\mu}^*)^\top (\boldsymbol{\zeta} - \boldsymbol{\zeta}^*), \end{aligned} \quad (20)$$

where  $\textcircled{1}$  follows from  $\nabla Q(\boldsymbol{\eta}) = \boldsymbol{\psi}(\boldsymbol{\eta})$  and  $\dot{\boldsymbol{\eta}} = \boldsymbol{\zeta}$  by definition. The equality  $\textcircled{2}$  follows from  $\boldsymbol{\mu} = \boldsymbol{\psi}(\boldsymbol{\eta})$  and  $\boldsymbol{\zeta}^* = \mathbf{0}$  in edge dynamics (2).

The time derivative of the Lyapunov function is

$$\begin{aligned}
& \dot{V}(\mathbf{x}, \boldsymbol{\eta}, \mathbf{s})|_{\mathbf{x}^*, \boldsymbol{\eta}^*, \mathbf{s}^*} \\
&= \sum_{i=1}^n \dot{W}_i^{\mathcal{V}}(x_i, x_i^*) + \dot{B}^{\mathcal{E}}(\boldsymbol{\eta}, \boldsymbol{\eta}^*) + \dot{B}^{\mathcal{V}}(\mathbf{s}, \mathbf{s}^*) \\
&\stackrel{\textcircled{1}}{\leq} - \sum_{i=1}^n \rho_i \|y_i - y_i^*\|^2 + (\mathbf{y} - \mathbf{y}^*)^\top (\mathbf{u} - \mathbf{u}^*) + (\boldsymbol{\mu} - \boldsymbol{\mu}^*)^\top (\boldsymbol{\zeta} - \boldsymbol{\zeta}^*) + (\mathbf{r}(\mathbf{s}) + \mathbf{r}(\mathbf{s}^*))^\top (-\mathbf{y} + \mathbf{y}^*) \\
&\stackrel{\textcircled{2}}{=} - \sum_{i=1}^n \rho_i \|y_i - y_i^*\|^2 + (\mathbf{y} - \mathbf{y}^*)^\top (\mathbf{p}(-\mathbf{y} + \mathbf{y}^*)) - (\mathbf{y} - \mathbf{y}^*)^\top \mathbf{E}(\boldsymbol{\mu} - \boldsymbol{\mu}^*) + (\boldsymbol{\zeta} - \boldsymbol{\zeta}^*)^\top (\boldsymbol{\mu} - \boldsymbol{\mu}^*) \\
&\stackrel{\textcircled{3}}{=} - \sum_{i=1}^n \rho_i \|y_i - y_i^*\|^2 + (\mathbf{y} - \mathbf{y}^*)^\top (\mathbf{p}(-\mathbf{y} + \mathbf{y}^*)) \\
&\stackrel{\textcircled{4}}{\leq} - \sum_{i=1}^n \rho_i \|y_i - y_i^*\|^2
\end{aligned} \tag{21}$$

where ① follows from the strict EIP property of nodes and equations derived in (19)-(20). The equality ② is derived by plugging in the controller design in (8a) where  $\mathbf{u} = -\mathbf{E}\boldsymbol{\mu} + \mathbf{p}(-\mathbf{y} + \bar{y}\mathbf{1}_n) + \mathbf{r}(\mathbf{s}) = -\mathbf{E}\boldsymbol{\mu} + \mathbf{p}(-\mathbf{y} + \mathbf{y}^*) + \mathbf{r}(\mathbf{s})$  and  $\mathbf{u}^* = -\mathbf{E}\boldsymbol{\mu}^* + \mathbf{p}(-\mathbf{y}^* + \bar{y}\mathbf{1}_n) + \mathbf{r}(\mathbf{s}^*) = -\mathbf{E}\boldsymbol{\mu}^* + \mathbf{p}(-\mathbf{y}^* + \mathbf{y}^*) + \mathbf{r}(\mathbf{s}^*)$ . The equality ③ uses the relation that  $-(\mathbf{y} - \mathbf{y}^*)^\top \mathbf{E}(\boldsymbol{\mu} - \boldsymbol{\mu}^*) = -(\mathbf{E}^\top (\mathbf{y} - \mathbf{y}^*))^\top (\boldsymbol{\mu} - \boldsymbol{\mu}^*) = -(\boldsymbol{\zeta} - \boldsymbol{\zeta}^*)^\top (\boldsymbol{\mu} - \boldsymbol{\mu}^*)$ . The inequality ④ uses  $(\mathbf{y} - \mathbf{y}^*)^\top (\mathbf{p}(-\mathbf{y} + \mathbf{y}^*)) = -\sum_{i=1}^n (p_i(y_i^* - y_i))(y_i^* - y_i) \leq 0$  since  $p_i(y_i^* - y_i)$  is the same sign with  $(y_i^* - y_i)$  by Controller Design 1.

Therefore,  $\dot{V}(\mathbf{x}, \boldsymbol{\eta}, \mathbf{s})|_{\mathbf{x}^*, \boldsymbol{\eta}^*, \mathbf{s}^*} \leq 0$  with equality only holds at the equilibrium. By Lyapunov stability theory in Proposition 1, the system is locally asymptotically stable around the equilibrium.

## B.2 Proof of Theorem 2

We start by showing that the design of the stacked-ReLU neural network forms a piece-wise linear function that is strictly increasing and across the origin. Then, we show the proof of its universal approximation property in Theorem 2.

Expanding the terms in the stacked-ReLU neural network gives

$$g(z) = \sum_{j=1}^d \alpha_j^+ \sigma(z - \beta_j^+) + \sum_{j=1}^d \alpha_j^- \sigma(-z + \beta_j^-) \tag{22a}$$

$$\text{where } -\infty < \sum_{j=1}^d \alpha_j^- < 0 < \sum_{j=1}^d \alpha_j^+ < \infty \tag{22b}$$

$$\beta_d^- \leq \dots \leq \beta_1^- = 0 = \beta_1^+ \leq \dots \leq \beta_d^+. \tag{22c}$$

Note that the neuron  $\alpha_j^+ \sigma(z - \beta_j^+) = \alpha_j^+ (z - \beta_j^+)$  if  $z \geq \beta_j^+$  (sometimes called activated) and equals to zero otherwise. Similarly, the neuron  $\alpha_j^- \sigma(-z + \beta_j^-) = \alpha_j^- (-z + \beta_j^-)$  if  $z \leq \beta_j^-$  and equals to zero otherwise. Hence, the constraint  $\beta_d^- \leq \dots \leq \beta_1^- = 0 = \beta_1^+ \leq \dots \leq \beta_d^+$  guarantees that the neurons activate in sequence such that

$$g(z) = \begin{cases} \sum_{j=1}^d \alpha_j^+ (z - \beta_j^+), & z > \beta_d^+ \\ \sum_{j=1}^k \alpha_j^+ (z - \beta_j^+), & z \in (\beta_k^+, \beta_{k+1}^+], \quad k = 1, \dots, d-1 \\ 0, & z = 0 \\ \sum_{j=1}^k \alpha_j^- (-z + \beta_j^-), & z \in [\beta_{k+1}^-, \beta_k^-), \quad k = 1, \dots, d-1 \\ \sum_{j=1}^d \alpha_j^- (-z + \beta_j^-), & z < \beta_d^-. \end{cases} \tag{23}$$

Hence,  $g(z)$  forms a piece-wise linear function across the origin, and constraints  $-\infty < \sum_{j=1}^d \alpha_j^- < 0 < \sum_{j=1}^d \alpha_j^+ < \infty$  further guarantee that the slope is positive, i.e., the function is strictly increasing. The proof of the universal approximation of monotonic functions in Theorem 2 is given as follows.

*Proof.* Let  $\mathcal{Z}$  be a closed interval in  $\mathbb{R}$  and  $r(z) : \mathcal{Z} \mapsto \mathbb{R}$  be a bounded,  $L$ -Lipschitz continuous and monotonically increasing function through the origin. First, we show that any  $r(z)$  can be approximated with bounded error by a piece-wise linear function with  $d$  pieces. Next, we show that the piece-wise linear function with  $d$  pieces can be constructed exactly using the stacked ReLU structure with  $d$  neurons.

Define an equispaced grid of points on  $\mathcal{Z}$ , where  $\tau = \frac{1}{d}$  is the spacing between grid points along each dimension. Corresponding to each grid interval  $[(k-1)\tau, k\tau]$  with  $k = 1, \dots, d$ , assign a linear function

$$\tilde{g}(z) = r((k-1)\tau) + \frac{r(k\tau) - r((k-1)\tau)}{\tau}(z - (k-1)\tau), \quad (24)$$

where  $\tilde{g}((k-1)\tau) = r((k-1)\tau)$  and  $\tilde{g}(k\tau) = r(k\tau)$ .

Since  $r(\cdot)$  is monotonic increasing, we have  $r((k-1)\tau) \leq r(z) \leq r(k\tau)$  and  $r((k-1)\tau) \leq \tilde{g}(z) \leq r(k\tau)$  for all  $z \in [(k-1)\tau, k\tau]$ . Therefore, we can bound the approximation error by

$$|\tilde{g}(z) - r(z)| \leq |r(k\tau) - r((k-1)\tau)| \leq L\tau, \quad (25)$$

where the last inequality follows from the  $L$ -Lipschitz continuous property of  $r(\cdot)$ .

Then, we show that any piece-wise linear function  $\tilde{g}(z)$  in (24) can be represented exactly using the monotone neural network constructed in (9). Without loss of generality, assume that  $z \geq 0$  and thus the function (9) is reduced to  $g(z) = \sum_{j=1}^d \alpha_j^+ \sigma(z - \beta_j^+)$ . Let  $\beta_k^+ = (k-1)\tau$ ,  $\sum_{j=1}^k \alpha_j^+ = \frac{r(k\tau) - r((k-1)\tau)}{\tau}$  for  $k = 1, 2, \dots, d$ . Then the construction of  $g(z)$  is exactly the same as  $\tilde{g}(z)$ . Therefore,  $|g(z) - r(z)|$  can also be bounded by  $L\tau$  using (25). We take  $\tau < \frac{\epsilon}{L}$  to complete the proof.  $\square$

### B.3 Proof of Lemma 1

*Proof.* We prove the equivalence of optimization by showing that the steady-state output  $\mathbf{y}^* = \bar{y}\mathbf{1}_n$  and only if  $\mathbf{k}_x^{-1}(\mathbf{h}^{-1}(\bar{y}\mathbf{1}_n)) = \mathbf{w}^* - \mathbf{E}\boldsymbol{\mu}^*$ . First, we show necessity. If  $\mathbf{y}^* = \bar{y}\mathbf{1}_n$ , the well-defined bijective mapping in assumption 2 gives the unique state  $\mathbf{x}^* = \mathbf{h}^{-1}(\bar{y}\mathbf{1}_n)$  and the unique input  $\mathbf{u}^* = \mathbf{k}_x^{-1}(\mathbf{h}^{-1}(\bar{y}\mathbf{1}_n))$ . We thus have  $\mathbf{u}^* = \mathbf{w}^* - \mathbf{E}\boldsymbol{\mu}^* = \mathbf{k}_x^{-1}(\mathbf{h}^{-1}(\bar{y}\mathbf{1}_n))$ . Next, we show sufficiency. If  $\mathbf{k}_x^{-1}(\mathbf{h}^{-1}(\bar{y}\mathbf{1}_n)) = \mathbf{w}^* - \mathbf{E}\boldsymbol{\mu}^*$ , we have  $\mathbf{u}^* = \mathbf{k}_x^{-1}(\mathbf{h}^{-1}(\bar{y}\mathbf{1}_n))$ . Then  $\mathbf{x}^* = \mathbf{k}_x(\mathbf{u}^*) = \mathbf{h}^{-1}(\bar{y}\mathbf{1}_n)$  and thus  $\mathbf{y}^* = \mathbf{h}(\mathbf{x}^*) = \bar{y}\mathbf{1}_n$ .

To prove the identical marginal costs, consider the Lagrangian function  $\mathcal{L}(\mathbf{w}, \boldsymbol{\mu}, \boldsymbol{\lambda}) = \sum_{i=1}^n C_i(w_i^*) + \boldsymbol{\lambda}^\top (\mathbf{k}_x^{-1}(\mathbf{h}^{-1}(\bar{y}\mathbf{1}_n)) - \mathbf{w}^* + \mathbf{E}\boldsymbol{\mu}^*)$ , where  $\boldsymbol{\lambda} \in \mathbb{R}^n$  is the multiplier. The KKT conditions [36] gives

$$\nabla_{\mathbf{w}^*} \mathcal{L}(\mathbf{w}^*, \boldsymbol{\mu}^*, \boldsymbol{\lambda}) = \nabla_{\mathbf{w}^*} C(\mathbf{w}^*) - \boldsymbol{\lambda} = \mathbf{0}_n \quad (26a)$$

$$\nabla_{\boldsymbol{\mu}^*} \mathcal{L}(\mathbf{w}^*, \boldsymbol{\mu}^*, \boldsymbol{\lambda}) = -\mathbf{E}^\top \boldsymbol{\lambda} = \mathbf{0}_n \quad (26b)$$

$$\nabla_{\boldsymbol{\lambda}} \mathcal{L}(\mathbf{w}^*, \boldsymbol{\mu}^*, \boldsymbol{\lambda}) = \mathbf{k}_x^{-1}(\mathbf{h}^{-1}(\bar{y}\mathbf{1}_n)) - \mathbf{w}^* + \mathbf{E}\boldsymbol{\mu}^* = \mathbf{0}_n \quad (26c)$$

By [37], the incidence matrix of a connected graph satisfy  $\mathcal{N}(\mathbf{E}^\top) = \text{range}\{\mathbf{1}\}$ . Hence, (26b) implies  $\boldsymbol{\lambda} \in \text{range}\{\mathbf{1}\}$  and (26a) further yields  $\nabla_{\mathbf{w}^*} C(\mathbf{w}^*) = \boldsymbol{\lambda} \in \text{range}\{\mathbf{1}\}$ . Moreover, (26c) is satisfied since  $\mathbf{w}^*$  and  $\boldsymbol{\mu}^*$  are variables at the equilibrium. Hence,  $\mathbf{w}^*$  solves (10) if and only if  $\nabla_{\mathbf{w}^*} C(\mathbf{w}^*) \in \text{range}\{\mathbf{1}\}$ .  $\square$

#### B.4 Proof of Lemma 2

*Proof.* We start by showing that  $\mathbf{r}(\mathbf{s})^T \hat{\mathbf{c}} \tilde{\mathbf{E}} \phi \left( \tilde{\mathbf{E}}^T \nabla \mathbf{C}(\mathbf{r}(\mathbf{s})) \right) \geq 0$  with equality holds if and only if  $\nabla \mathbf{C}(\mathbf{r}(\mathbf{s})) \in \text{range}(\mathbf{1}_n)$ . Expanding the left side of (13) and pre-multiplying  $\mathbf{r}(\mathbf{s})$  gives

$$\begin{aligned} & \mathbf{r}(\mathbf{s})^T \left( \hat{\mathbf{c}} \tilde{\mathbf{E}} \phi \left( \tilde{\mathbf{E}}^T \nabla \mathbf{C}(\mathbf{r}(\mathbf{s})) \right) \right) \\ &= \sum_{l=(i,j) \in \tilde{\mathcal{E}}} \phi_l \left( \nabla C_i(r_i(s_i)) - \nabla C_j(r_j(s_j)) \right) (c_i r_i(s_i) - c_j r_j(s_j)) \\ &= \sum_{l=(i,j) \in \tilde{\mathcal{E}}} \phi_l \left( \nabla C_o(c_i r_i(s_i)) - \nabla C_o(c_j r_j(s_j)) \right) (c_i r_i(s_i) - c_j r_j(s_j)) \end{aligned} \quad (27)$$

where the last step follows from the cost function in Assumption 3 that  $\nabla C_i(r_i(s_i)) = \nabla C_o(c_i r_i(s_i))$  for all  $i \in \mathcal{V}$ .

Since  $C_o(\cdot)$  is strictly convex, its gradient  $\nabla C_o(\cdot)$  is strictly increasing [36]. Thus,

$$\left( \nabla C_o(c_i r_i(s_i)) - \nabla C_o(c_j r_j(s_j)) \right) (c_i r_i(s_i) - c_j r_j(s_j)) \geq 0, \quad (28)$$

with equality holds if and only if  $\nabla C_o(c_i r_i(s_i)) = \nabla C_o(c_j r_j(s_j))$ .

By controller Design 2,  $\phi_l \left( \nabla C_o(c_i r_i(s_i)) - \nabla C_o(c_j r_j(s_j)) \right)$  is the same sign with  $\nabla C_o(c_i r_i(s_i)) - \nabla C_o(c_j r_j(s_j))$ . Hence, (28) implies

$$\phi_l \left( \nabla C_o(c_i r_i(s_i)) - \nabla C_o(c_j r_j(s_j)) \right) (c_i r_i(s_i) - c_j r_j(s_j)) \geq 0$$

with equality holds if and only if  $\nabla C_o(c_i r_i(s_i)) = \nabla C_o(c_j r_j(s_j))$ . This implies  $\nabla C_i(r_i(s_i)) = \nabla C_j(r_j(s_j)) \forall l = (i, j) \in \tilde{\mathcal{E}}$  for cost functions satisfying Assumption 3. Since the communication graph is connected, we further have  $\nabla C_1(r_1(s_1)) = \dots = \nabla C_n(r_n(s_n))$ , i.e.,  $\nabla \mathbf{C}(\mathbf{r}(\mathbf{s})) \in \text{range}(\mathbf{1}_n)$ .

Then we prove that  $\hat{\mathbf{c}} \tilde{\mathbf{E}} \phi \left( \tilde{\mathbf{E}}^T \nabla \mathbf{C}(\mathbf{r}(\mathbf{s})) \right) = \mathbf{0}_n$  if and only if  $\nabla \mathbf{C}(\mathbf{r}(\mathbf{s})) \in \text{range}(\mathbf{1}_n)$  by showing sufficiency and necessity. If  $\nabla \mathbf{C}(\mathbf{r}(\mathbf{s})) \in \text{range}(\mathbf{1}_n)$ , we have  $\tilde{\mathbf{E}}^T \nabla \mathbf{C}(\mathbf{r}(\mathbf{s})) = \mathbf{0}_n$  and thus  $\hat{\mathbf{c}} \tilde{\mathbf{E}} \phi \left( \tilde{\mathbf{E}}^T \nabla \mathbf{C}(\mathbf{r}(\mathbf{s})) \right) = \mathbf{0}_n$ . On the other hand, if  $\hat{\mathbf{c}} \tilde{\mathbf{E}} \phi \left( \tilde{\mathbf{E}}^T \nabla \mathbf{C}(\mathbf{r}(\mathbf{s})) \right) = \mathbf{0}_n$ . Multiplying both sides by  $\mathbf{r}(\mathbf{s})^T$  gives  $\mathbf{r}(\mathbf{s})^T \hat{\mathbf{c}} \tilde{\mathbf{E}} \phi \left( \tilde{\mathbf{E}}^T \nabla \mathbf{C}(\mathbf{r}(\mathbf{s})) \right) = 0$  and therefore  $\nabla \mathbf{C}(\mathbf{r}(\mathbf{s})) \in \text{range}(\mathbf{1}_n)$ . Hence,  $\hat{\mathbf{c}} \tilde{\mathbf{E}} \phi \left( \tilde{\mathbf{E}}^T \nabla \mathbf{C}(\mathbf{r}(\mathbf{s})) \right) = \mathbf{0}_n$  if and only if  $\nabla \mathbf{C}(\mathbf{r}(\mathbf{s})) \in \text{range}(\mathbf{1}_n)$ .  $\square$

#### B.5 Proof of Theorem 3

We first show that suppose the closed-loop system (1)-(2) has a feasible equilibrium, the equilibrium is unique with output agreement  $\mathbf{y}^* = \bar{y} \mathbf{1}_n$ . Then, we prove that the system is locally asymptotically stable around the equilibrium.

The derivation of the equilibrium and its uniqueness is given as follows.

*Proof.* At the equilibrium, we have  $\mathbf{f}(\mathbf{x}^*, \mathbf{u}^*) = \mathbf{0}$  and  $\zeta^* = \mathbf{0}$ . For a connected graph, the null space of  $\mathbf{E}^T$  is  $\mathcal{N}(\mathbf{E}^T) = \text{range} \{ \mathbf{1}_n \}$  [37]. Using  $\zeta^* = \mathbf{E}^T \mathbf{y}^* = \mathbf{0}$ , we have  $\mathbf{y}^* = \hat{y} \mathbf{1}_n$ . The right side of (12b) equals to zero at the equilibrium gives  $(\hat{y} \mathbf{1}_n - \bar{y} \mathbf{1}_n) = -\hat{\mathbf{c}} \mathbf{E} \phi \left( \mathbf{E}^T \nabla \mathbf{C}(\mathbf{r}(\mathbf{s})) \right)$ . Multiplying both sides by  $\mathbf{1}_n^T \hat{\mathbf{c}}^{-1}$  yields  $(\hat{y} - \bar{y}) \mathbf{1}_n^T \hat{\mathbf{c}}^{-1} \mathbf{1}_n = -\mathbf{1}_n^T \mathbf{E} \phi \left( \mathbf{E}^T \nabla \mathbf{C}(\mathbf{r}(\mathbf{s})) \right)$ , which equals to zero since  $\mathbf{1}_n^T \mathbf{E} = \mathbf{0}_n$  for a connected graph. This implies  $\hat{y} = \bar{y}$  since  $\mathbf{1}_n^T \hat{\mathbf{c}}^{-1} \mathbf{1}_n > 0$  for  $\hat{\mathbf{c}} \succ \mathbf{0}$ . Therefore,  $\mathbf{y}^* = \bar{y} \mathbf{1}_n$  and thus  $\mathbf{x}^* = \mathbf{h}^{-1}(\bar{y} \mathbf{1}_n)$  by bijective mapping of  $\mathbf{h}(\cdot)$ .

Moreover,  $\mathbf{y}^* = \bar{y} \mathbf{1}_n$  implies  $\hat{\mathbf{c}} \tilde{\mathbf{E}} \phi \left( \tilde{\mathbf{E}}^T \nabla \mathbf{C}(\mathbf{r}(\mathbf{s}^*)) \right) = \mathbf{0}_n$ . By Lemma 2,  $\nabla \mathbf{C}(\mathbf{r}(\mathbf{s})) \in \text{range}(\mathbf{1}_n)$  and thus there exists a scalar  $\gamma$  such that  $\nabla C_i(r_i(s_i^*)) = \gamma$  for all  $i \in \mathcal{V}$ . This implies  $\nabla C_o(c_i r_i(s_i^*)) = \gamma$  by Assumption 3. The strict convexity of  $C_o(\cdot)$  implies that  $\nabla C_o(\cdot)$  is a strictly increasing function, which guarantees the existence of  $\nabla C_o^{-1}(\cdot)$  that is also a strictly increasing function [38]. Hence,  $r_i(s_i^*) = \nabla C_o^{-1}(\gamma) c_i^{-1}$  and compactly we have  $\mathbf{r}(\mathbf{s}^*) = \nabla C_o^{-1}(\gamma) \hat{\mathbf{c}}^{-1} \mathbf{1}_n$ .



From the bijective mapping of  $\mathbf{k}_x(\cdot)$ ,  $\mathbf{u}^* = \mathbf{k}_x^{-1}(\mathbf{x}^*) = \mathbf{k}_x^{-1}(\mathbf{h}^{-1}(\bar{y}\mathbb{1}_n))$ . From  $\mathbf{p}(-\mathbf{y}^* + \bar{y}\mathbb{1}_n) = \mathbb{0}_n$ , we have  $\mathbf{u}^* = -\mathbf{E}\boldsymbol{\mu}^* + \mathbf{r}(\mathbf{s}^*)$  and therefore  $-\mathbf{E}\boldsymbol{\mu}^* = \mathbf{k}_x^{-1}(\mathbf{h}^{-1}(\bar{y}\mathbb{1}_n)) - \nabla C_o^{-1}(\gamma)\hat{\mathbf{c}}^{-1}\mathbb{1}_n$ . Since  $\mathbb{1}_n^\top \mathbf{E}\boldsymbol{\mu}^* = 0$ , we have  $\nabla C_o^{-1}(\gamma) = -(\mathbb{1}_n^\top \mathbf{k}_x^{-1}(\mathbf{h}^{-1}(\bar{y}\mathbb{1}_n))) / (\sum_{i=1}^n c_i^{-1})$ . The uniqueness of  $\gamma$  is guaranteed by the strict increasing property of function  $\nabla C_o^{-1}(\gamma)$ . Similarly, the uniqueness of  $\mathbf{s}^*$  satisfying  $\mathbf{r}(\mathbf{s}^*) = \nabla C_o^{-1}(\gamma)\hat{\mathbf{c}}^{-1}\mathbb{1}_n$  is guaranteed by the strict increasing property of function  $r_i(\cdot)$  for  $i \in \mathcal{V}$ .

Then, we prove the uniqueness of  $\boldsymbol{\eta}^*$  by contradiction. By  $\boldsymbol{\mu}^* = \boldsymbol{\psi}(\boldsymbol{\eta}^*)$ , we have  $-\mathbf{E}\boldsymbol{\psi}(\boldsymbol{\eta}^*) = \mathbf{k}_x^{-1}(\mathbf{h}^{-1}(\bar{y}\mathbb{1}_n)) - \nabla C_o^{-1}(\gamma)\hat{\mathbf{c}}^{-1}\mathbb{1}_n$ . Suppose there is  $\hat{\boldsymbol{\eta}} \in \mathbb{R}^m$  and  $\hat{\boldsymbol{\eta}} \neq \boldsymbol{\eta}^*$  such that  $\mathbf{E}\boldsymbol{\psi}(\boldsymbol{\eta}^*) = \mathbf{E}\boldsymbol{\psi}(\hat{\boldsymbol{\eta}})$ . Since  $\boldsymbol{\eta} \in \mathcal{R}(\mathbf{E}^\top)$ , there exist  $\mathbf{z}^* \in \mathbb{R}^n$  and  $\hat{\mathbf{z}} \in \mathbb{R}^n$  such that  $\boldsymbol{\eta}^* = \mathbf{E}^\top \mathbf{z}^*$  and  $\hat{\boldsymbol{\eta}} = \mathbf{E}^\top \hat{\mathbf{z}}$ . Then  $(\mathbf{z}^* - \hat{\mathbf{z}})^\top (\mathbf{E}\boldsymbol{\psi}(\boldsymbol{\eta}^*) - \mathbf{E}\boldsymbol{\psi}(\hat{\boldsymbol{\eta}})) = (\mathbf{z}^* - \hat{\mathbf{z}})^\top (\mathbf{E}\boldsymbol{\psi}(\mathbf{E}^\top \mathbf{z}^*) - \mathbf{E}\boldsymbol{\psi}(\mathbf{E}^\top \hat{\mathbf{z}})) = \sum_{l=(i,j) \in \mathcal{E}} (z_{ij}^* - \hat{z}_{ij}) (\psi_l(z_{ij}^*) - \psi_l(\hat{z}_{ij}))$ . Since  $\psi_l(\cdot)$  is monotonically increasing, we have  $(z_{ij}^* - \hat{z}_{ij}) (\psi_l(z_{ij}^*) - \psi_l(\hat{z}_{ij})) \geq 0$  for all  $l$  with equality only holds when  $z_{ij}^* = \hat{z}_{ij}$  (which is equivalent to  $\mathbf{E}^\top \mathbf{z}^* = \mathbf{E}^\top \hat{\mathbf{z}}$  and thus  $\boldsymbol{\eta}^* = \hat{\boldsymbol{\eta}}$ ). Hence,  $\mathbf{E}\boldsymbol{\psi}(\boldsymbol{\eta}^*) = \mathbf{E}\boldsymbol{\psi}(\hat{\boldsymbol{\eta}})$  in and only if  $\boldsymbol{\eta}^* = \hat{\boldsymbol{\eta}}$ .  $\square$

Next, we prove that the equilibrium is asymptotically stable by the same Lyapunov function (18) in the proof of Theorem 1. The proof is given as follows.

*Proof.* Different from (19), the time derivative of  $B^\mathcal{V}(\mathbf{s}, \mathbf{s}^*)$  is

$$\begin{aligned} \dot{B}^\mathcal{V}(\mathbf{s}, \mathbf{s}^*) &= (\nabla L(\mathbf{s}) - \nabla L(\mathbf{s}^*))^\top \dot{\mathbf{s}} \\ &\stackrel{\textcircled{1}}{=} (\mathbf{r}(\mathbf{s}) + \mathbf{r}(\mathbf{s}^*))^\top \left( -(\mathbf{y} - \mathbf{y}^*) - \hat{\mathbf{c}}\tilde{\mathbf{E}}\boldsymbol{\phi} \left( \tilde{\mathbf{E}}^\top \nabla C(\mathbf{r}(\mathbf{s})) \right) \right), \end{aligned} \quad (29)$$

where  $\textcircled{1}$  follows from  $\nabla L(\boldsymbol{\eta}) = \mathbf{r}(\mathbf{s})$  and  $\dot{\mathbf{s}} = \left( -(\mathbf{y} - \mathbf{y}^*) - \hat{\mathbf{c}}\tilde{\mathbf{E}}\boldsymbol{\phi} \left( \tilde{\mathbf{E}}^\top \nabla C(\mathbf{r}(\mathbf{s})) \right) \right)$  by Controller Design 2.

The time derivative of the Lyapunov function in (18) is

$$\begin{aligned} \dot{V}(\mathbf{x}, \boldsymbol{\eta}, \mathbf{s})|_{\mathbf{x}^*, \boldsymbol{\eta}^*, \mathbf{s}^*} &= \sum_{i=1}^n \dot{W}_i^\mathcal{Y}(x_i, x_i^*) + \dot{B}^\mathcal{E}(\boldsymbol{\eta}, \boldsymbol{\eta}^*) + \dot{B}^\mathcal{V}(\mathbf{s}, \mathbf{s}^*) \\ &\stackrel{\textcircled{1}}{\leq} - \sum_{i=1}^n \rho_i \|y_i - y_i^*\|^2 + (\mathbf{y} - \mathbf{y}^*)^\top (\mathbf{u} - \mathbf{u}^*) + (\boldsymbol{\mu} - \boldsymbol{\mu}^*)^\top (\boldsymbol{\zeta} - \boldsymbol{\zeta}^*) \\ &\quad + (\mathbf{r}(\mathbf{s}) + \mathbf{r}(\mathbf{s}^*))^\top \left( -(\mathbf{y} - \mathbf{y}^*) - \hat{\mathbf{c}}\tilde{\mathbf{E}}\boldsymbol{\phi} \left( \tilde{\mathbf{E}}^\top \nabla C(\mathbf{r}(\mathbf{s})) \right) \right) \\ &\stackrel{\textcircled{2}}{=} - \sum_{i=1}^n \rho_i \|y_i - y_i^*\|^2 + (\mathbf{y} - \mathbf{y}^*)^\top (\mathbf{p}(-\mathbf{y} + \mathbf{y}^*)) - (\mathbf{y} - \mathbf{y}^*)^\top \mathbf{E}(\boldsymbol{\mu} - \boldsymbol{\mu}^*) + (\boldsymbol{\zeta} - \boldsymbol{\zeta}^*)^\top (\boldsymbol{\mu} - \boldsymbol{\mu}^*) \\ &\quad + (\mathbf{r}(\mathbf{s}) + \mathbf{r}(\mathbf{s}^*))^\top \left( -\hat{\mathbf{c}}\tilde{\mathbf{E}}\boldsymbol{\phi} \left( \tilde{\mathbf{E}}^\top \nabla C(\mathbf{r}(\mathbf{s})) \right) \right) \\ &\stackrel{\textcircled{3}}{=} - \sum_{i=1}^n \rho_i \|y_i - y_i^*\|^2 + (\mathbf{y} - \mathbf{y}^*)^\top (\mathbf{p}(-\mathbf{y} + \mathbf{y}^*)) + (\mathbf{r}(\mathbf{s}) + \mathbf{r}(\mathbf{s}^*))^\top \left( -\hat{\mathbf{c}}\tilde{\mathbf{E}}\boldsymbol{\phi} \left( \tilde{\mathbf{E}}^\top \nabla C(\mathbf{r}(\mathbf{s})) \right) \right) \\ &\stackrel{\textcircled{4}}{=} - \sum_{i=1}^n \rho_i \|y_i - y_i^*\|^2 + (\mathbf{y} - \mathbf{y}^*)^\top (\mathbf{p}(-\mathbf{y} + \mathbf{y}^*)) - \mathbf{r}(\mathbf{s})^\top \left( \hat{\mathbf{c}}\tilde{\mathbf{E}}\boldsymbol{\phi} \left( \tilde{\mathbf{E}}^\top \nabla C(\mathbf{r}(\mathbf{s})) \right) \right) \\ &\stackrel{\textcircled{5}}{\leq} - \sum_{i=1}^n \rho_i \|y_i - y_i^*\|^2 \end{aligned} \quad (30)$$

where  $\textcircled{1}$  follows from the strict EIP of nodes dynamics and (19)-(20). The equality  $\textcircled{2}$  is derived by plugging in the controller design in (8a) where  $\mathbf{u} = -\mathbf{E}\boldsymbol{\mu} + \mathbf{p}(-\mathbf{y} + \bar{y}\mathbb{1}_n) + \mathbf{r}(\mathbf{s})$  and  $\mathbf{u}^* = -\mathbf{E}\boldsymbol{\mu}^* + \mathbf{p}(-\mathbf{y}^* + \bar{y}\mathbb{1}_n) + \mathbf{r}(\mathbf{s}^*) = -\mathbf{E}\boldsymbol{\mu}^* + \mathbf{r}(\mathbf{s}^*)$ . The equality  $\textcircled{3}$  uses the relation that  $-(\mathbf{y} - \mathbf{y}^*)^\top \mathbf{E}(\boldsymbol{\mu} - \boldsymbol{\mu}^*) = -(\mathbf{E}^\top (\mathbf{y} - \mathbf{y}^*))^\top (\boldsymbol{\mu} - \boldsymbol{\mu}^*) = -(\boldsymbol{\zeta} - \boldsymbol{\zeta}^*)^\top (\boldsymbol{\mu} - \boldsymbol{\mu}^*)$ . The equality

④ follows from  $\mathbf{r}(\mathbf{s}^*)^\top \hat{\mathbf{c}} \tilde{\mathbf{E}} \phi \left( \tilde{\mathbf{E}}^\top \nabla \mathbf{C}(\mathbf{r}(\mathbf{s})) \right) = \nabla C_o^{-1}(\gamma) \mathbb{1}_n^\top (\hat{\mathbf{c}}^{-1})^\top \hat{\mathbf{c}} \tilde{\mathbf{E}} \phi \left( \tilde{\mathbf{E}}^\top \nabla \mathbf{C}(\mathbf{r}(\mathbf{s})) \right) = \nabla C_o^{-1}(\gamma) \mathbb{1}_n^\top \tilde{\mathbf{E}} \phi \left( \tilde{\mathbf{E}}^\top \nabla \mathbf{C}(\mathbf{r}(\mathbf{s})) \right) = 0$  since  $\mathbb{1}_n^\top \tilde{\mathbf{E}} = 0$ . The inequality ⑤ uses  $(\mathbf{y} - \mathbf{y}^*)^\top (\mathbf{p}(-\mathbf{y} + \mathbf{y}^*)) = -\sum_{i=1}^n (p_i(y_i^* - y_i))(y_i^* - y_i) \leq 0$  since  $p_i(y_i^* - y_i)$  is the same sign with  $(y_i^* - y_i)$  by Controller Design 1, and  $\mathbf{r}(\mathbf{s})^\top \left( \hat{\mathbf{c}} \tilde{\mathbf{E}} \phi \left( \tilde{\mathbf{E}}^\top \nabla \mathbf{C}(\mathbf{r}(\mathbf{s})) \right) \right) \geq 0$  shown in Lemma 2.

Therefore,  $\dot{V}(\mathbf{x}, \boldsymbol{\eta}, \mathbf{s})|_{\mathbf{x}^*, \boldsymbol{\eta}^*, \mathbf{s}^*} \leq 0$  with equality only holds at the equilibrium. By Lyapunov stability theory in Proposition 1, the system is locally asymptotically stable around the equilibrium.  $\square$

## C Experiments

We demonstrate the effectiveness the proposed neural-PI control in two networked systems: vehicle platooning and power system frequency control. All experiments are run with a NVIDIA Tesla P100 GPU with 16GB memory. The neural PI controller can be trained by any model-based or model-free algorithms, and we use the RNN-based framework in [6, 33] for training. For completeness, the figures highlighted in Section 5 are also shown below with more thorough discussions.

### C.1 Vehicle Platooning

The first experiment is the vehicle platoon control in Figure 1(b). We adopt the model in [2, 4] with the following assumptions: (i) the drivers are heterogeneous and have different "preferred" velocities, (ii) the influence between vehicles is bi-directional, and (iii) the set of neighbors to a vehicle is not changing over time.

Let  $\mathcal{V}$  be the set of all the vehicles. The vehicle  $i \in \mathcal{V}$  adjusts its velocity  $x_i$  according to its preferred velocities  $V_i^0 > 0$  and its sensitivities  $V_i^1 > 0$  to the distance from neighbouring vehicles. The dynamic model is  $\dot{x}_i = \kappa_i \left( -(x_i - V_i^0 - u_i^v) + V_i^1 u_i^e \right)$  where  $\kappa_i > 0$  is a constant,  $u_i^v$  is the adjustment of preferred velocities and  $u_i^e$  is the adjustment depends on the relative position to its neighbours. The neighbouring vehicles are described by edges  $\mathcal{E}$ . If vehicle  $i$  neighbours vehicle  $j$  and  $i$  is in front of  $j$ , we associate an edge indexed by  $l$  for the relative position with  $i$  as the head and  $j$  as the tail. The relation of  $l = (i, j) \in \mathcal{E}$  is described by the incidence matrix  $\mathbf{E} \in \mathbb{R}^{n \times m}$ , where  $[\mathbf{E}]_{i,l}$  has value +1 if  $i$  is the head of edge  $l$ , and -1 if it is the tail, and 0 otherwise.

Let  $\tau_i$  be the position of vehicle  $i \in \mathcal{V}$ . For each  $l = (i, j) \in \mathcal{E}$ ,  $\eta_l = \tau_i - \tau_j$  denotes the relative position of vehicles  $i$  and  $j$ . The input  $u_i^e$  to each vehicle affected by all the neighbours is

$$u_i^e := -\sum_{l=1}^m [\mathbf{E}]_{i,l} \psi_l(\eta_l), \quad (31)$$

where  $\psi_l(\cdot)$  is the feedback function of the relative position indexed by edge  $l$ . The physical meaning is as follows. If a vehicle is the tail of  $l$  and finds that the relative position  $\eta_l$  is larger, then the vehicle tends to increase the speed such that it would be more closer to the front neighbours. On the other hand, if a vehicle is the head of  $l$  and notice that the relative position  $\eta_l$  is larger, then the vehicle tends to decrease the speed such that the rear vehicles would not fall behind too far.

The vehicle platoon needs to reach an agreement of the same velocity to avoid potential collisions. Denote a change of variable with  $w_i = V_i^1 u_i^v$  and  $u_i = u_i^e + w_i$ . The vehicle platoon control can be represented in the standard form (1)-(2). The node dynamics can be identified as

$$\mathcal{V}_i: \quad \dot{x}_i = \kappa_i \left( -(x_i - V_i^0) + V_i^1 u_i \right), \quad y_i = x_i, \quad (32)$$

with the output  $y_i$  being the velocity  $x_i$ .

By physical law,  $\dot{\tau}_i = x_i$  and thus  $\dot{\eta}_l = \dot{\tau}_i - \dot{\tau}_j = x_i - x_j$ . The edge dynamics can be identified as

$$\mathcal{E}_l: \quad \dot{\eta}_l = \zeta_l, \quad \mu_l = \psi_l(\eta_l), \quad (33)$$

where the input  $\zeta_l$  is the relative velocity  $x_i - x_j$  and the output  $\mu_l$  is the position feedback  $\psi_l(\eta_l)$ .

In a vector form, the inputs of the nodes (31) affected by the the edge feedbacks are written as  $\mathbf{u}^e = -\mathbf{E}\boldsymbol{\mu}$ . The inputs of the edges impacted by the nodes are written as  $\boldsymbol{\zeta} = \mathbf{E}^\top \mathbf{y}$ . This recovers the input-output coupling of nodes and edges shown in Figure 1.

**Verification of Assumptions 1-2.** We start by checking assumptions 1-2 to show that the proposed controller design works for this networked system.

*Well defined bijective mapping.* For the node dynamics (32),  $f_i(x_i, u_i) = \kappa_i (-(x_i - V_i^0) + V_i^1 u_i)$  and  $h_i(x_i) = x_i$ , where  $h_i(\cdot)$  is obviously a bijective mapping. At the equilibrium,  $f_i(x_i^*, u_i^*) = 0$  gives  $-(x_i^* - V_i^0) + V_i^1 u_i^* = 0$ . This yields a well-defined bijective mapping  $k_{x,i}(u_i^*) = V_i^1 u_i^* + V_i^0$ ,  $k_{y,i}(u_i^*) = V_i^1 u_i^* + V_i^0$ . The corresponding inverse function of  $h_i(\cdot)$  and  $k_{x,i}(\cdot)$  are  $h_i^{-1}(y_i^*) = y_i^*$  and  $k_{x,i}^{-1}(x_i^*) = (x_i^* - V_i^0)/V_i^1$ , respectively.

*Strict EIP of node dynamics.* The well defined bijective mapping  $k_{x,i}(\cdot)$  guarantees that for every  $u_i^* \in \mathcal{U}_i^*$ , there exists a unique  $x_i^* \in \mathcal{X}$  such that  $f_i(x_i^*, u_i^*) = 0$ . Let the storage function be  $W_i^{\mathcal{V}}(x_i, x_i^*) = \frac{1}{2\kappa_i V_i^1} (x_i - x_i^*)^2$ . Then

$$\begin{aligned} W_i^{\mathcal{V}}(x_i, x_i^*) &= \frac{1}{\kappa_i V_i^1} (x_i - x_i^*) \dot{x}_i \\ &= \frac{1}{V_i^1} (x_i - x_i^*) (-(x_i - V_i^0) + V_i^1 u_i) \\ &\stackrel{\textcircled{1}}{=} -\frac{1}{V_i^1} (x_i - x_i^*)^2 + (x_i - x_i^*) (u_i - u_i^*) \\ &\stackrel{\textcircled{2}}{=} -\frac{1}{V_i^1} (y_i - y_i^*)^2 + (y_i - y_i^*) (u_i - u_i^*) \end{aligned}$$

where  $\textcircled{1}$  follows from  $-(x_i^* - V_i^0) + V_i^1 u_i^* = 0$  and  $\textcircled{2}$  follows from  $y_i = x_i$  by definition. Since  $V_i^1 > 0$ , each node dynamics (32) is strictly EIP with  $\rho_i = \frac{1}{V_i^1}$  and the storage function  $W_i^{\mathcal{V}}(x_i, x_i^*)$ .

**Design Freedom.** The first design freedom is the edge feedback function  $\psi_l(\cdot)$ . By Controller Design 1, we aim to design the function  $\psi_l(\cdot)$  to be monotonically increasing such that the system is asymptotically stable and synchronous to the agreement level.

The second design freedom is the adjustments to the preferred velocity by  $w_i$ . Let  $\tilde{C}_i(u_i^v) : \mathbb{R} \mapsto \mathbb{R}$  be the cost on the deviation  $u_i^v$  of the preferred velocities. We would like to maintain at the required velocity  $\bar{y}$  at the lowest cost  $\sum_{i \in \mathcal{V}} \tilde{C}_i(u_i^v)$ . Let  $C_i(w_i) := \tilde{C}_i(V_i^1 w_i) = \tilde{C}_i(u_i^v)$ . The objective function of the steady-state resource allocation is then equivalent to  $\sum_{i \in \mathcal{V}} C_i(w_i)$ .

### C.1.1 Simulation and Visualization

**Simulation Setup** We adopt the parameter setup in [2, 4] for the dynamic traffic model. The number of vehicles is  $n = 20$  and is placed on a line graph. The sensitivity parameter is  $\kappa_i = 1$  for all vehicles. The parameters  $V_i^0$  and  $V_i^1$  are randomly generated by  $V_i^0 \sim \text{uniform}[5, 6]$  and  $V_i^1 \sim \text{uniform}[0.5, 1]$ , respectively. We generate the training and test set of size 300 with initial velocities  $x_i(0) \sim \text{uniform}[5, 6]$ . The state  $\eta_l$  is initialized as 2 and  $s_i$  is initialized as 0, respectively. The stepsize between time states is set as  $\Delta t = 0.02s$  and the number of time stages in a trajectory in the training set is  $K = 300$ . The communication graph is randomly generated to be a regular graph with degree three. The episode number and batch size are 400 and 300, respectively.

**Learning Edge Feedback Function.** We first demonstrate the performance of the learned edge feedback function  $\psi_l(\cdot)$ , for systems without external control  $w$ . Controller Design 1 provides the algebraic constraint on the function  $\psi(\cdot)$  to be strictly increasing. This condition is also presented in [2, 4] for networked system without external control. These works, however, did not consider how to choose a good  $\psi(\cdot)$ . The functions  $\psi_l(\eta_l) = \tanh(\eta_l)$  and  $\psi_l(\eta_l) = (\eta_l)^{1/3}$  are used in [4] and [2], respectively. In this paper, we parameterize the function  $\psi(\cdot)$  using the monotone neural network design in (9). The loss function in training is set to be  $J(\mathbf{y}) = \sum_{i=1}^n \left( \sum_{k=200}^K |y_i(k\Delta t) - \frac{1}{n} \sum_{j=1}^n y_j(k\Delta t)| \right) + \sum_{l=1}^m \text{relu}(-\eta_l + 1)$ , which penalizes on the speed disagreement in the last 100 steps and the relative distance smaller than 1. This loss function is used to encourage quicker convergence and avoid potential collisions caused by too small distances. We adopt a trick to add a small regularization on edge feedback parameterized by  $0.01 \sum_{l=1}^m \sum_{k=1}^K \mu_i(k\Delta t)^2$  to avoid oscillations caused by too large slope.

Figure 5 compares the performance of  $\psi_l(\cdot)$  parameterized by neural networks (labeled as StableNN) with  $\tanh(\eta_l - \eta_0)$  in [4] and  $(\eta_l - \eta_0)^{1/3}$  (labeled as poly1/3) in [2], where  $\eta_0 = 2$  is the initial distance of neighbouring vehicles. The shape of different edge feedback functions is shown in Figure 2(a), where StableNN learns a monotonically increasing function with flexible shapes. Figure 2(b)-(d) visualize the transient velocity of all vehicles from the same initial condition. All of the dynamics reach an output agreement at approximate 5.6 without external control  $w$ , with StableNN realizes better transient performance with quick convergence.

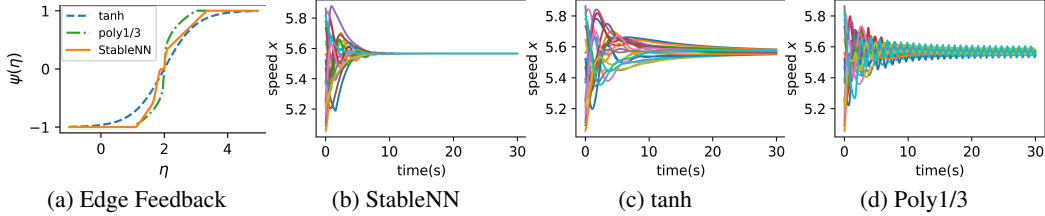


Figure 5: (a) Comparison of the edge feedback functions learned by StableNN with tanh and poly1/3. (b)-(c) Dynamics of the system with the three edge feedback functions. All of the dynamics reach an agreement, with StableNN converges quickest.

**Controller Performances.** We implement external control law in  $w$  to realize a specific output agreement at 5.2 and reduce steady-state allocation cost. The transient cost is set to be  $J(\mathbf{y}, \mathbf{w}) = \sum_{i=1}^n \sum_{k=1}^{300} |y_i(k\Delta t) - \bar{y}| + c_i(w_i(k\Delta t))^2$ , where  $c_i \sim \text{uniform}[0.025, 0.075]$ . The steady-state cost in resource allocation (4) is  $C(\mathbf{w}) = \sum_{i=1}^n c_i(w_i^*)^2$ , where we use  $w_i(20)$  to approximate  $w_i^*$  since the dynamics approximately enter the steady state after  $t = 15s$  as we will show later in simulation. The loss function in training is set to be the same as  $J(\mathbf{y}, \mathbf{w})$ , such that neural networks are optimized to reduce transient cost through training.

We compare the performance of the learned structured neural-PI controllers, 1) StableNN-Comm, the neural-PI controller with communication (Controller design 2) and, 2) StableNN-WoComm, the neural-PI controller without communication (Controller Design 1). Both neural-PI controllers are parameterized by monotone neural networks given in Theorem 2, where the number of neurons in the hidden layer is  $d = 20$ . The neural networks are updated using Adam with learning rate initializes at 0.05 and decays every 50 steps with a base of 0.7. We compare against two benchmarks with communication: 3) DenseNN-Comm: Two-layer dense neural networks with ReLU activation, and the number of neurons in the hidden layer is 20. The neural networks are updated using Adam with learning rate initializes at 0.007 and decays every 100 steps with a base of 0.7. Note that DenseNN needs such a small learning rate to let the training converge, the reason is that DenseNN may lead to unstable behaviors that we will see later. 4) Linear-Comm: Conventional PI control parameterized by  $p_i(\bar{y}_i - y_i) = \theta_{i,1}(\bar{y}_i - y_i)$  and  $r(s_i) = \theta_{i,2}s_i$ , where  $\theta_{i,1} \in \mathbb{R}$  and  $\theta_{i,2} \in \mathbb{R}$  are linear coefficients optimized through learning. The coefficients are updated using Adam with learning rate initializes at 0.05 and decays every 50 steps with a base of 0.7.

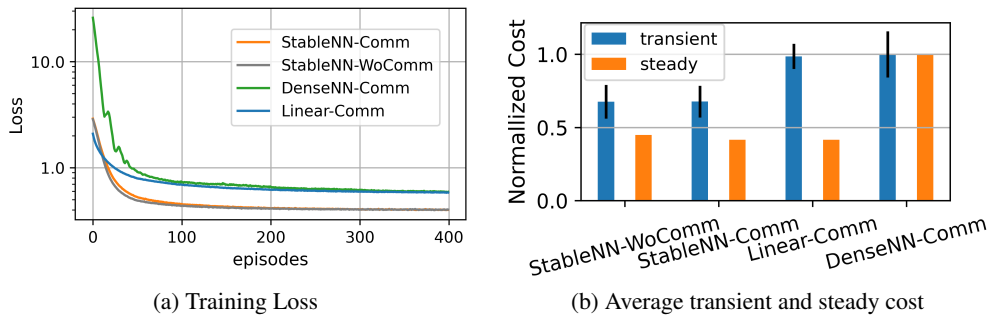


Figure 6: (a) Average batch loss along episodes. All converges, with the StableNN achieves the lowest cost. (b) The average transient cost and steady-state cost with error bar on the randomly generated test set with size 300. StableNN achieves transient cost that is much lower than others. Comm-StableNN and Comm-Linear lead to the same lowest steady-state cost guaranteed by Controller Design 2.

The average batch loss during episodes of training is shown in Figure 6(a). All of the four methods converge, with the StableNN achieves the lowest cost. Figure 6(b) shows the transient and steady-state cost on the test set. The transient cost is aligned with the observations in the training loss, where StableNN achieves transient cost that is much lower than others. StableNN-Comm and Linear-Comm have the lowest possible steady-state cost, as guaranteed by Theorem 3. By contrast, DenseNN-Comm without structured design has both high cost in transient and steady-state performances.

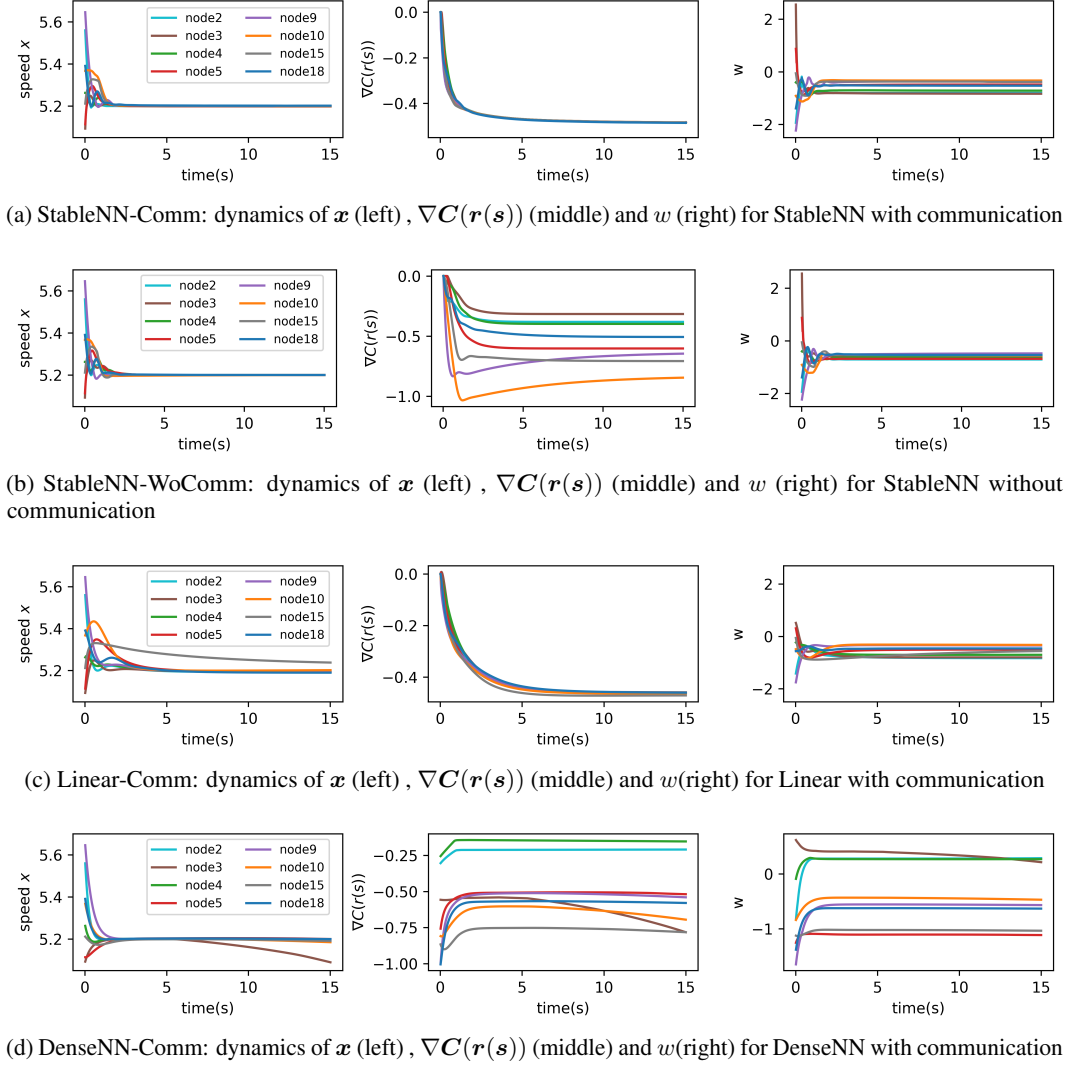


Figure 7: Dynamics of the system under four methods on 8 nodes with the required output agreement  $\bar{y} = 5.2$ . (a) StableNN-Comm achieves the output agreement level and identical marginal cost. (b) StableNN-WoComm achieves the output agreement but fail to converge to the identical-marginal-cost solution. (c) Linear-Comm is stable but has slower convergence compared with neural network-based approaches. (d) DenseNN-Comm leads to unstable behavior in node 3.

Figure 7 shows the dynamics of velocity speed  $\boldsymbol{x}$ , marginal cost  $\nabla C(\boldsymbol{r}(s))$  and external control action  $w$  on 8 nodes under the four methods. As guaranteed by Controller Design 2, StableNN-Comm in Figure 7(a) reaches the same speed at 5.2 and identical marginal cost, indicating that it achieves the required output agreement level with the lowest resource allocation cost. StableNN-WoComm in Figure 7(b) also reaches the required output agreement level guaranteed by Controller Design 1. However, the marginal cost converges at different levels for different nodes because of the lack of communication. Linear-Comm is stable and converges to the solution with identical marginal cost, but it has slower convergence compared with neural network-based approaches. Even through DenseNN-Comm achieves finite loss both in training and testing, node 3 in Figure 7(d) actually

exhibits unstable behaviors. Hence, the four controllers exhibit qualitatively different behaviors even though they both achieve finite training losses in Figure 6. It is necessary to enforce stability and steady-state optimally constraints on controller design to achieve performance guarantees.

## C.2 Power Systems Frequency Control

The model of power systems reflects the transmission of electricity from generators to loads through power transmission lines. The power system is naturally a physical network with a typical topology shown in Figure 8. Let  $\mathcal{V}$  be the set of all the synchronous generators and  $\mathcal{E}$  be the set of transmission lines. For each generator  $i \in \mathcal{V}$ , the rotating speed (i.e., frequency)  $x_i$  changes with the mismatch between power generation and consumption. We aim to maintain the real-time balance of power generation and consumption by controlling the frequency of all generators at the same nominal value  $\bar{x}$  (e.g., 60Hz in the US).

Let  $P_i^m$  denote the fixed power generation and  $\Delta P_i^m$  denote the adjustable power generation (e.g., batteries). Let  $P_i^e$  be the power injection from the connected transmission lines and  $d_i$  be the load at the node  $i$ . Then the mismatch between power generation and consumption is  $(P_i^m + \Delta P_i^m) + P_i^e - d_i$ . We adopt a commonly used model that assumes the bus voltage magnitudes are maintained at the nominal level and the reactive power flows are ignored, which is suitable to frequency control of transmission systems with small resistances and well-regulated voltages [24, 39]. The frequency dynamic of node  $i \in \mathcal{V}$  is represented as

$$\dot{x}_i = -\rho_i(x_i - \bar{x}) + (P_i^m + \Delta P_i^m) + P_i^e - d_i,$$

where  $\rho_i$  is the damping constant corresponding to the physical system. Note that the load  $d_i$  is time-varying. In particular, power system operator emphasizes on the ability of the system to withstand a big disturbance such as a step load change. Such ability is quantified by the maximum frequency deviation and its convergence to the nominal frequency after step load changes.

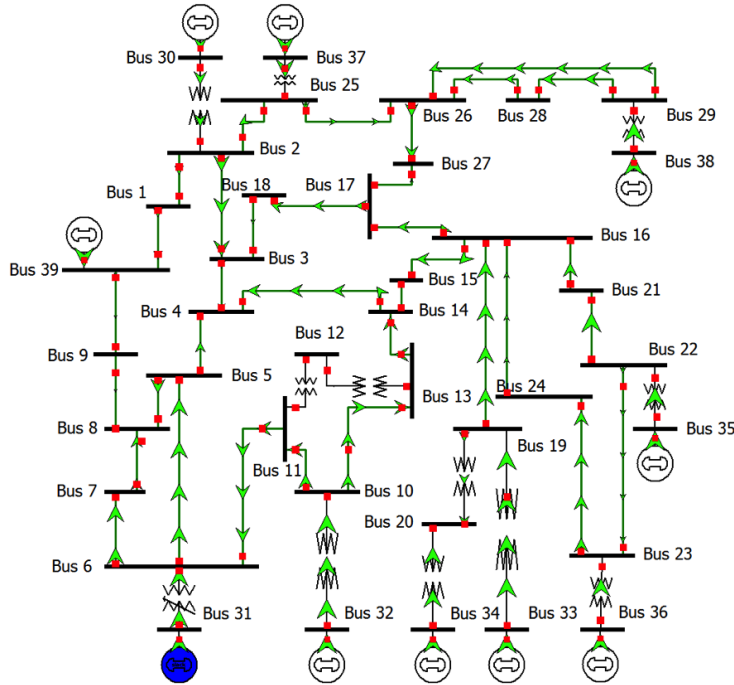


Figure 8: IEEE 39-bus test system [34]

The term  $P_i^e$  follows the physical law of power flow in the transmission network. We usually designate a positive direction of the power flow in the transmission line for convenience. Let  $\mu_l$  be the power flow in the positive direction of the edge  $l$ . If the transmission line  $l$  connects nodes  $i$  and  $j$  and we designate the power flow from  $i$  to  $j$  as the positive direction, then the incidence matrix  $\mathbf{E} \in \mathbb{R}^{n \times m}$

associated with the edge  $l = (i, j) \in \mathcal{E}$  is described elementwise as  $[\mathbf{E}]_{i,l} = +1$ ,  $[\mathbf{E}]_{j,l} = -1$  and  $[\mathbf{E}]_{k,l} = 0$  for  $k \neq i, j$ . By this definition, the electricity injection from transmission lines to the node  $i$  is  $P_i^e = -\sum_{l=1}^m [\mathbf{E}]_{i,l} \mu_l$ . In a vector form, we have  $\mathbf{P}^e = -\mathbf{E}\boldsymbol{\mu}$ .

Denote a change of variable such that  $w_i = \Delta P_i^m$  and  $u_i = \Delta P_i^m + P_i^e$ , then the power system frequency control problem can be represented in the standard form (1)-(2). The node dynamics can be identified as

$$\mathcal{V}_i: \quad \dot{x}_i = -\rho_i(x_i - \bar{x}) + P_i^m - d_i + u_i, \quad u_i = w_i - \sum_l E_{il} \mu_l, \quad y_i = x_i. \quad (34)$$

By physical law, the active power flow in the line  $l = (i, j)$  is affected by the angle differences between node  $i$  and  $j$ . Let  $\delta_i$  be the angle of the node  $i$ . The state of the line  $l = (i, j) \in \mathcal{E}$  is the angle difference  $\eta_l = \delta_i - \delta_j$  and correspondingly,  $\dot{\eta}_l = \dot{\delta}_i - \dot{\delta}_j = x_i - x_j$ . The power flow is  $\mu_l = b_l \sin(\delta_i - \delta_j)$  by the Kirchhoff's circuit laws [24, 39], where  $b_l$  is a constant representing the susceptance of the transmission line. Thus, the dynamics of the edge is represented by

$$\mathcal{E}_l: \quad \dot{\eta}_l = \zeta_l, \quad \zeta_l = x_i - x_j, \quad \mu_l = b_l \sin(\eta_l). \quad (35)$$

In a vector form, we have  $\boldsymbol{\zeta} = \mathbf{E}^\top \mathbf{y}$ . This together with  $\mathbf{P}^e = -\mathbf{E}\boldsymbol{\mu}$  recovers the input-output coupling of nodes and edges shown in Fig. 1.

Unlike the vehicle platooning problem, we cannot change the feedback function  $\mu_l = b_l \sin(\eta_l)$  in the edge dynamics because of the physical law. Here, we optimize  $\mathbf{w}$  such that the frequency reaches the nominal value at the steady state and the cost of power generation is minimized.

**Verification of Assumptions 1-2.** We start by checking assumptions 1-2 to show that the proposed controller design works for this networked system.

*Well defined bijective mapping.* For the node dynamics (32),  $f_i(x_i, u_i) = -\rho_i(x_i - \bar{x}) + P_i^m - d_i + u_i$  and  $h_i(x_i) = x_i$ , where  $h_i(\cdot)$  is obviously a bijective mapping. At the equilibrium,  $f_i(x_i^*, u_i^*) = 0$  gives  $-\rho_i(x_i^* - \bar{x}) + P_i^m - d_i + u_i^* = 0$ . This yields a well-defined bijective mapping  $k_{x,i}(u_i^*) = \bar{x} + (P_i^m - d_i + u_i^*)/\rho_i$ ,  $k_{y,i}(u_i^*) = \bar{x} + (P_i^m - d_i + u_i^*)/\rho_i$ . The corresponding inverse function of  $h_i(\cdot)$  and  $k_{x,i}(\cdot)$  are  $h_i^{-1}(y_i^*) = y_i^*$  and  $k_{x,i}^{-1}(x_i^*) = \rho_i(x_i^* - \bar{x}) + d_i - P_i^m$ , respectively.

*Strict EIP of node dynamics.* The well defined bijective mapping  $k_{x,i}(\cdot)$  guarantees that for every equilibrium  $u_i^* \in \mathcal{U}_i^*$ , there exists a unique  $x_i^* \in \mathcal{X}$  such that  $f_i(x_i^*, u_i^*) = 0$ . Let the storage function be  $W_i^{\mathcal{V}}(x_i, x_i^*) = \frac{1}{2}(x_i - x_i^*)^2$ . Then

$$\begin{aligned} W_i^{\mathcal{V}}(x_i, x_i^*) &= (x_i - x_i^*)\dot{x}_i \\ &= (x_i - x_i^*)(-\rho_i(x_i - \bar{x}) + P_i^m - d_i + u_i) \\ &\stackrel{\textcircled{1}}{=} -\rho_i(x_i - x_i^*)^2 + (x_i - x_i^*)(u_i - u_i^*) \\ &\stackrel{\textcircled{2}}{=} -\rho_i(y_i - y_i^*)^2 + (y_i - y_i^*)(u_i - u_i^*) \end{aligned}$$

where  $\textcircled{1}$  follows from the equilibrium  $(-\rho_i(x_i^* - \bar{x}) + P_i^m - d_i + u_i^*) = 0$  and  $\textcircled{2}$  follows from  $y_i = x_i$  by definition. Since  $\rho_i > 0$ , each node dynamics (32) is strictly EIP with  $\rho_i$  and the storage function  $W_i^{\mathcal{V}}(x_i, x_i^*)$

*Strictly increasing of edge feedback functions.* We adopt a common assumption in literature that the power system operates with angle differences  $\eta_l$  in the range  $\mathcal{H} = \{\eta | \eta_l \in (-\pi/2, \pi/2) \forall l \in \mathcal{E}\}$ , which is sufficiently large to include almost all practical scenarios [40, 41, 24]. Since  $\sin(\eta_l)$  is strictly monotonically increasing in  $(-\pi/2, \pi/2)$ , the conditions on strictly increasing of edge feedback functions are satisfied.

**Optimal Resource Allocation (Economic Dispatch).** Here we show an explicit derivation for the optimal resource allocation problem in (10). We aim to reach the output agreement such that  $\bar{y} = \bar{x}$ . Note that  $\mathbf{h}^{-1}(\bar{y}\mathbb{1}_n) = \bar{y}\mathbb{1}_n$  and  $\mathbf{k}_{x,i}^{-1}(\bar{y}) = \rho_i(\bar{x} - \bar{x}) + d_i - P_i^m = d_i - P_i^m$ , we have  $\mathbf{k}_x^{-1}(\mathbf{h}^{-1}(\bar{y}\mathbb{1}_n)) = \mathbf{k}_x^{-1}(\bar{y}\mathbb{1}_n) = \mathbf{d} - \mathbf{P}^m$ .

Then the constraint (10b) is written as  $\mathbf{d} = \mathbf{w}^* - \mathbf{E}\boldsymbol{\mu}^* + \mathbf{P}^m$ , which is the power balance equation at each node. Namely, the power consumption equals to the power injection at each node. The

optimization problem (4) is then written as

$$\min_{\mathbf{w}^*, \boldsymbol{\mu}^*} \sum_{i=1}^n C_i(w_i^*), \quad (36a)$$

$$\text{s.t. } \mathbf{d} = \mathbf{w}^* - \mathbf{E}\boldsymbol{\mu}^* + \mathbf{P}^m, \quad (36b)$$

which is the well-known economic dispatch problem in power systems that aims to serve power consumption with lowest cost in power generation [41, 40].

It is obvious that different  $\mathbf{d}$  affects the constrains (36b) and thus changes the optimal solution to the resources allocation. Since the loads are time-varying, one important benefit of the proposed approach is that it distributedly attain the optimal solution following the changes of the load levels without a centralized dispatch.

### C.2.1 Simulation and Visualization

**Simulation Setup** We conduct experiment on the IEEE New England 10-machine 39-bus (NE39) power network shown in Figure 8 with parameters given in [34, 6]. We generate the training and test set of size 300 by randomly picking at most three generators to have a step load change uniformly distributed in  $\text{uniform}[-1, 1]$  p.u., where 1p.u.=100 MW is the base unit of power for the IEEE-NE39 test system. Note that the load  $d_i$  is a parameter in the node dynamic (34), this experiment verifies the robustness of the controller under parameter changes. The state  $\eta_l$  is initialized as the solution of power flow at the nominal frequency and  $s_i$  is initialized as 0, respectively. The communication graph is randomly generated to be a regular graph with degree three. The episode number and batch size are 600 and 300, respectively. The stepsize between time states is set as  $\Delta t = 0.01s$  and the number of time stages in a trajectory in the training set is  $K = 400$ .

**Controller Performances.** We implement external control law in  $\mathbf{w}$  to realize the agreement of frequency at 60Hz and reduce steady-state power generation cost. Apart from the accumulated frequency deviation, an important metric for the frequency control problem is the maximum frequency deviation (also know as the frequency nadir) after a disturbance happens [6]. Hence, the transient cost is set to be  $J(\mathbf{y}, \mathbf{w}) = \sum_{i=1}^n \left( \max_{k=1, \dots, K} |y_i(k\Delta t) - \bar{y}| + 0.05 \sum_{k=1}^K |y_i(k\Delta t) - \bar{y}| + \sum_{k=1}^K c_i(w_i(k\Delta t))^4 \right)$ , where  $c_i \sim \text{uniform}[0.25, 0.75]$ . The steady-state cost in resource allocation (4) is  $C(\mathbf{w}) = \sum_{i=1}^n c_i(w_i^*)^4$ , where we use  $w_i(30)$  to approximate  $w_i^*$  since the dynamics approximate enter the steady state after  $t = 30s$  as we will show later in simulation. We use the cost function with the power of four to demonstrate that the proposed approach is not restricted to quadratic cost functions. The loss function in training is set to be  $J(\mathbf{y}, \mathbf{w})$ , such that neural networks are optimized to reduce transient cost through training.

We compare the performance of the learned structured neural-PI controllers, 1) StableNN-Comm, the neural-PI controller with communication (Controller design 2) and, 2) StableNN-WoComm, the neural-PI controller without communication (Controller Design 1). Both neural-PI controllers are parameterized by monotone neural networks given in Theorem 2, where the number of neurons in the hidden layer is  $d = 20$ . The neural networks are updated using Adam with learning rate initializes at 0.05 and decays every 50 steps with a base of 0.7. We compare against two benchmarks with communication: 3) DenseNN-Comm: Two-layer dense neural networks with ReLU activation, and the number of neurons in the hidden layer is 20. The neural networks are updated using Adam with learning rate initializes at 0.0015 and decays every 50 steps with a base of 0.7. Note that DenseNN needs such a small learning rate to let the training converge, the reason is that DenseNN easily lead to unstable behaviors that we will see later. 4) Linear-Comm: Conventional PI control parameterized by  $p_i(\bar{y}_i - y_i) = \theta_{i,1}(\bar{y}_i - y_i)$  and  $r(s_i) = \theta_{i,2}s_i$ , where  $\theta_{i,1} \in \mathbb{R}$  and  $\theta_{i,2} \in \mathbb{R}$  are linear coefficients optimized through learning. The trainable coefficients are updated using Adam with learning rate initializes at 0.05 and decays every 50 steps with a base of 0.7.

The average batch loss during episodes of training is shown in Figure 9(a). All of the four methods converge, with the StableNN achieves the lowest cost. Figure 9(b) shows the transient and steady-state costs on the test set. The transient cost is aligned with the observations in the training loss, where StableNN achieves transient cost that is much lower than others. Note that the load changes lead to different solutions of optimal resource allocation problem (36), thus the steady-state cost also has a



distribution shown in the error bar. Still, stableNN-Comm and Linear-Comm have the lowest possible steady-state cost, as guaranteed by Theorem 3. By contrast, DenseNN-Comm without structured design has both high cost in transient and steady-state performance.

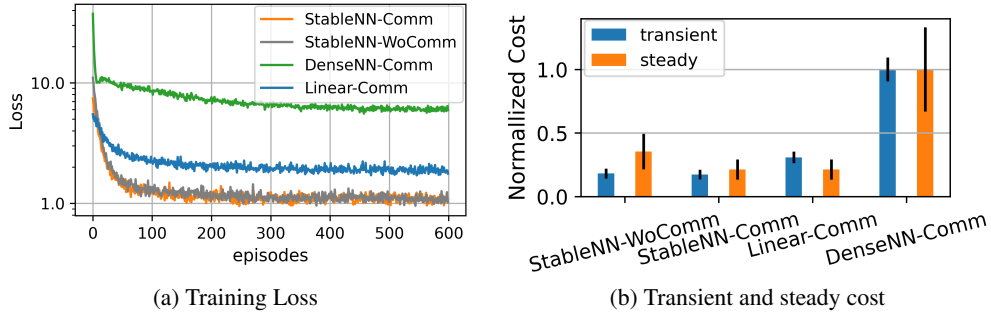
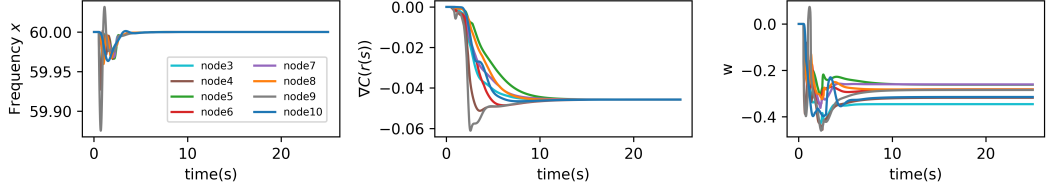
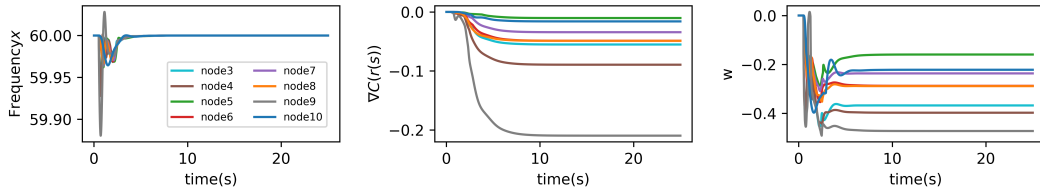


Figure 9: (a) Average batch loss along episodes. All converges, with the StableNN achieves the lowest cost. (b) The average transient cost and steady-state cost with error bar on the randomly generated test set with size 300. StableNN achieves transient cost that is much lower than others. StableNN-Comm and Linear-Comm lead to the same lowest steady-state cost guaranteed by Controller Design 2.

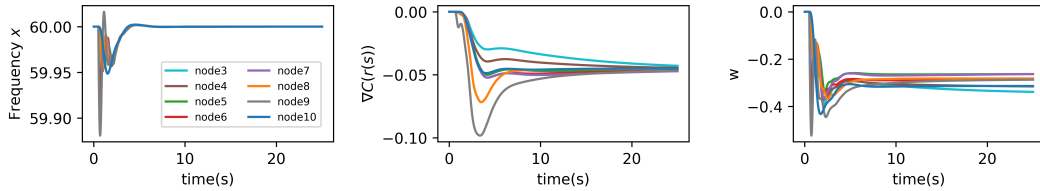
Figure 10 shows the dynamics of frequency  $x$ , marginal cost  $\nabla C(r(s))$  and external control action  $w$  on 8 nodes under the four methods. As guaranteed by Controller Design 2, StableNN-Comm in Figure 10(a) achieves the output agreement at 60Hz and identical marginal cost, indicating that it achieves the lowest resource allocation cost. StableNN-WoComm in Figure 10(b) also reaches the output agreement at 60Hz guaranteed by Controller Design 1. However, the marginal cost converges at different levels for different nodes because of the lack of communication. Linear-Comm in Figure 10(c) is also stable and converges to the solution with identical marginal cost, but it has slower convergence compared with neural network-based approaches. Even through DenseNN-Comm achieves finite loss both in training and testing, Figure 10(d) exhibits unstable behavior with large oscillations. Hence, the proposed Controller Design 1 and Controller Design 2 guarantee the stability criteria robust to parameter changes. Controller Design 2 further realizes economic dispatch of generators under different load levels distributedly.



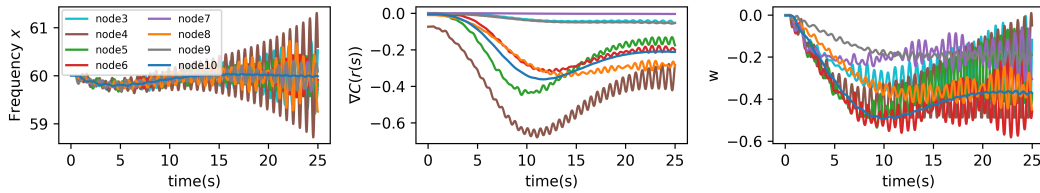
(a) StableNN-Comm: dynamics of  $\boldsymbol{x}$  (left),  $\nabla C(\boldsymbol{r}(s))$  (middle) and  $w$  (right) for StableNN with communication



(b) StableNN-WoComm: dynamics of  $\boldsymbol{x}$  (left),  $\nabla C(\boldsymbol{r}(s))$  (middle) and  $w$  (right) for StableNN without communication



(c) Linear-Comm: dynamics of  $\boldsymbol{x}$  (left),  $\nabla C(\boldsymbol{r}(s))$  (middle) and  $w$  (right) for Linear with communication



(d) DenseNN-Comm: dynamics of  $\boldsymbol{x}$  (left),  $\nabla C(\boldsymbol{r}(s))$  (middle) and  $w$  (right) for DenseNN with communication

Figure 10: Dynamics of the system under four methods on 8 nodes with the required output agreement  $\bar{y} = 60$ . (a) StableNN-Comm achieves the output agreement at 60Hz and identical marginal cost. (b) StableNN-WoComm achieves the output agreement but fail to converge to the identical-marginal-cost solution. (c) Linear-Comm is stable but has slower convergence compared with neural network-based approaches. (d) DenseNN-Comm leads to large frequency deviations and oscillations .